Fabrication of flexible self-charging power cell by integration of piezoelectric- triboelectric nanogenerator and reduced graphene oxide coated fabric supercapacitor

Final report

By

Asst. Dr. Viyada Harnchana

Department of Physics, Khon Kaen University

The Thailand Research Fund for New Scholar (MRG 2559)

Acknowledgement

This work was supported by the Thailand research fund. I would like to thank you Assoc. Prof. Dr. Vittaya Amornkitbamrung for his helpful guidance and kind support, and Prof. Dae Joon Kang for all his supervision, encouragement and knowledgeable suggestion.

Abstract

The flexible self-charging power cell (SCPC) was developed by the integration of piezoelectric with triboelectric nanogenerator and reduced graphene oxide (rGO) coated fabric supercapacitor. Polyvinylidene difluoride (PVDF)-ZnO film was used as a piezoelectric separator. The rGO supercapacitor electrodes were prepared by dip-coating graphene oxide on carbon fabric and thermally reduced to form rGO-coated fiber flexible electrodes. The top surface of electrode of the supercapacitor electrode was coated by a mixture of polydimethylsiloxane (PDMS) and GO (PDMS+GO) to form a single electrode triboelectric operation on the top part of the device. A self-charging power cell was assembled by separating two electrodes; the rGO and PDMS+GO/RGO electrodes, with PVA-H3PO4 gel electrolyte coated PVDF-ZnO piezoelectric separator. Using this configuration, the synergetic process of piezoelectric and triboelectric nanogenerators is expected to generate superior power output and self-charging performance of the SCPC. This outcome of this project would be beneficial for the fabrication of low cost, flexible and high performance self-charging power cells.

Keywords : Self- charging power cell; Piezoelectric; triboelectric Nanogenerator; graphene oxide

บทคัดย่อ

โครงงานวิจัยนี้ได้ทำการพัฒนาเซลล์พลังงานแบบชาร์จตัวเองได้โดยอาศัยการทำงานของแหล่งกำเนิดไฟฟ้านาโนแบบเพียโซอิเล็กทริกและทริโบอิเล็กทริกร่วมกับตัวเก็บประจุยิ่งยวดที่เคลือบบนผ้า แหล่งกำเนิดไฟฟ้านาโนแบบเพียโซอิเล็กทริกประดิษฐ์จากฟิล์มของคอมโพสิต Polyvinylidene difluoride (PVDF) และ ZnO ซึ่งทำหน้าที่เป็น separator ของตัวเก็บประจุ ขั้วอิเล็กโทรดของตัวเก็บประจุยิ่งยวดทำขึ้นจากการเคลือบแกรฟีนออกไซด์ (Graphene oxide (GO)) ลงบนผ้าคาร์บอนและทำการรีดิวส์ด้วยการเผาให้ความร้อนเพื่อให้กลายเป็น (reduced graphene oxide (rGO)) ขั้วอิเล็กโทรดด้านบนของตัวเก็บประจุแบบยิ่งยวดนั้นถูกเคลือบด้วยฟิล์มคอมโพสิตของ polydimethylsiloxane (PDMS) และ GO เพื่อเป็นทำหน้าที่เป็นแหล่งกำเนิดไฟฟ้านาโนแบบทริโบอิเล็กทริกในการทำงานแบบ single electrode เซลล์พลังงานแบบชาร์จตัวเองได้นี้ประกอบขึ้นจากสองขั้วอิเล็กโทรด ซึ่งได้แก่ขั้ว rGO และขั้ว PDMS+GO/RGO และใช้อิเล็กโทรไลท์แบบเจล PVA-H3PO4 ซึ่งเคลือบบนฟิล์ม PVDF-ZnO piezoelectric separator ด้วยโครงสร้างของเซลล์พลังงานนี้ ในการใช้วัสดุเพียโซ่อิเล็กทริกและทริโบอิเล็กทริกในแหล่งกำเนิดไฟฟ้านาโน นั้นคาดว่าจะสามารถเก็บเกี่ยวพลังงานเชิงกลเป็นพลังงานไฟฟ้าและได้เซลล์พลังงานไฟฟ้าประสิทธิภาพสูงได้ ผลลัพธ์จากงานวิจัยนี้จะเป็นประโยชน์ในการผลิตเซลล์พลังงานไฟฟ้าแบบชาร์จตัวเองได้ที่มีประสิทธิภาพสูงและมีต้นทุนการผลิตต่ำ

Executive Summary

The main contribution of this work is the facile, straightforward fabrication of a high-performance negative triboelectric material composed of polydimethylsiloxane (PDMS), graphene oxide (GO), and sodium dodecyl sulfate (SDS). We believe that this contribution is theoretically and practically relevant because the output voltage and current of the composite film were three times higher than those of the pristine PDMS film in a pilot triboelectric nanogenerator. Our research is of particular interest and use to materials scientists in the field of energy harvesting devices. Further, the SDS surfactant and GO which was partially reduced in situ synergistically intensified the negative charge density, and the GO also provided enhanced charge trapping, thus improving the performance of the PDMS triboelectric film. The outcome of this work would be beneficial for the fabrication of the development of flexible and high performance self-charging power cells.

Content

Figures

Tables

List of Publications

1. Viyada Harnchana, Van Huynh Ngoc, Wen He, Aamir Rashhed, Hyunje Park, Vittaya Amornkitbamrung, and Dae Joon Kang, Enhanced Power Output of a Triboelectric Nanogenerator using Polydimethylsiloxane Modified with Graphene Oxide and Sodium Dodecyl sulfate, ACS applied materials and interfaces, article ASAP (2018) (IF=8.097) [published online on 6 July 2018]

Chapter 1

Introduction

Harvesting the ubiquitous mechanical energy in ambient environment is one of the most demanding challenges in developing green, sustainable energy sources. Triboelectric nanogenerators (TENGs) are newly developed energy conversion devices with high potential as a power generation technology because of their high output power and cost-effective fabrication.[1-3] The electric power generation of TENGs is based on triboelectrification and electric induction, which depend on the contact–separation movements of the two triboelectric materials with different triboelectric polarities.[4] Triboelectric materials are coupled according to the large difference in their electronegativities, as presented in the triboelectric series in Figure 1.1a) [3, 5]. To realize their practical applications, high-performance flexible and wearable TENGs need to be developed. And four basic operation modes are proposed for the mechanical energy in various systems[6].

Self-charging powered cell (SCPC) is a great desired concept for developing next generation portable electronic devices that integrates an energy conversion device with energy storage device. One of the effective energy conversion devices typically employed in SCPC system is nanogenerator that harvest mechanical energy from human living environment through piezoelectric and tribo-electrification effects and covert into electricity. On the other hand, energy storage devices including supercapacitors or Li-ion battery store electricity as electrochemical energy. These two systems are generally two dependent processes which require separated physical units.

Positive			Negative
	Polyformaldehyde 1.3-1.4	(continued)	
	Etylcellulose	Polyester (Dacron)	
	Polyamide 11	Polyisobutylene	
	Polyamide 6-6	Polyuretane flexible sponge	
	Melanime formol	Polyethylene Terephthalate	
	Wool, knitted	Polyvinyl butyral	
	Silk, woven	Polychlorobutadiene	
	Aluminum	Natural rubber	
	paper	Polyacrilonitrile	
	Cotton, woven	Acrylonitrile-vinyl chloride	
	Steel	Polybisphenol carbonate	
	Wood	Polychloroether	
	Hard rubber	Polyvinylidine chloride (Saran)	
	Nickel, copper	Polystyrene	
	Sulfur	Polyethylene	
	Brass, silver	Polypropylene	
	Acetate, Rayon	Polyimide (Kapton)	
	Polymethyl methacrylate (Lucite)	Polyvinyl Chloride (PVC)	
	Polyvinyl alcohol	Polydimethylsiloxane (PDMS)	
	(continued)	Polytetrafluoroethylene (Teflon)	

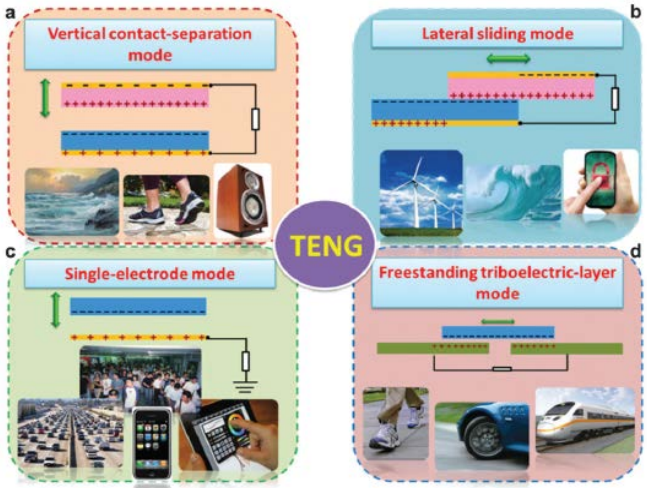

Figure 1.1 a) Triboelectric series[3], b) four basic operation modes of triboelectric nanogenerators [6]

In recent years, a new hybrid system that integrates energy conversion and energy storage device to perform a self-charging powered operation in order to directly convert mechanical energy into electrochemical energy in one single device has been introduced. Many self-charging powered cells (SCPCs) have been developed including the hybrid systems of piezoelectric nanogenerator and either Li batteries [7-11] or supercapacitor [12]. Additionally, wearable electronics are currently of considerable interest and have been found in many applications such as personalized electronics, wearable medical monitors and

military field [13]. Textile based SCPC integrated into wearable garments to harvest the energy from body movement and directly stored would be one of important challenges. The possibility of producing flexible self-powered electronic devices was first addressed where a flexible self-charging supercapacitor power cell (SCSPC) has been successfully developed [12]. In this device, a polyvinylidene difluoride (PVDF) - ZnO film was used as a piezoelectric nanogenerator and MnO2 nanowires as electrode material for supercapacitor with the use of PVA/H_3PO_4 gel electrolyte. However, the device performances were still far less than those of the typical stand-alone nanogenerator and supercapacitor.

In a typical SCPC, piezoelectric potential is created in nanogenerator by mechanical deformation which can drive electrolyte ions migration causing charging reactions at the electrodes. This charging process occurs through a periodic applied strain. The piezoelectric film is therefore a primary components that plays a crucial role in the generating the high enough potential energy to drive this charging process to occur.

Poly(vinylidene fluoride) (PVDF) film is a piezoelectric material (β-phase PVDF) which has a high piezoelectric coefficient, excellent stability under deformation and has been used in many flexible nanogenerator designs for mechanical harvesting [7-11, 14] . ZnO-based piezoelectric nanogenerators are one of the most important candidates for developing self-powered nanotechnology because of its wurtzite structure that could generate spontaneous polarization along that direction. Moreover, ZnO also offer many advantages such as low-cost, environmental friendliness and low temperature with large scale production [15].

In this proposal, PVDF-ZnO nanowires will be used as piezoelectric material in nanogerator for flexible SCPC. In addition, graphene oxide (GO) based triboelectric nanogenerator (TENG) will be integrated in order to enhance the energy harvesting

performance of the produced SCPC. TENG is a new developed nanogenerator that can convert mechanical energy into electricity by using triboelectrification and electrostatic induction which offers many advantages including extremely high output and efficiency, low cost, high stability and environmental friendliness [1, 3]. The detail of TENG is described in the literature review.

Another crucial part is to store the harvested energy into energy storage device. Supercapacitors offer many appealing aspects including high power density, fast charge-discharge rates and long life times compared to rechargeable batteries and conventional dielectric capacitors. MnO_2 has been known to be promising electrode materials because of their low cost, environmental friendliness, and high theoretical capacitance of up to 1400 Fg^{-1} [16]. However, commercial MnO_2 exhibits a specific capacitance of only ~ 200 Fg^{-1} because of the limited electroactive area and poor electrical conductivity [17, 18]. For these reason, to get the high capacitive performance, mixing with carbon or other conductive material and binder agent is always required to fabricate supercapacitor electrodes. Finding high capacitance, high flexibility, cost - effective and binder-free supercapacitor electrode materials would be very useful for the development of wearable and flexible SCPC.

Graphene has been known for its excellent electrical conductivity, large surface area and high mechanical flexibility, which are appealing for electric double-layer capacitor electrode material for supercapacitor applications. The theoretical specific capacitance of 550 Fg^{-1} could be achieved from graphene based supercapacitor [19], which is relatively low compared to that of MnO_2. However, graphene produced by chemical method or reduced graphene oxide (rGO) offers many advantages including a large scale cost-effective fabrication and a good dispersibility in many solvents due to its hydrophilic nature enabling it easily deposited on various kinds of substrates. A binder-free thermally reduced graphene oxide-coated fabric electrode for a flexible solid-state supercapacitor has been demonstrated

with a high device capacitance of 70.4 Fg^{-1} [20]. Moreover, graphene oxide (GO) is insulating material which is also ideal for tribielectric nanogenerator application which would be beneficial for enhancing the energy conversion efficiency due to an improved power output as a result of a combination of piezoelectric and triboelectric effects.

To sum up, this research is going to develop a wearable and flexible SCPC with enhanced performance involving the fabrication of a hybrid SCPC between piezoelectric-triboelectric nanogenerator and solid state supercapacitor. The device will compose two rGO coated conducting fabric supercapacitor electrodes, a piezoelectric PVDF-ZnO as a separator which coated with PVA-H3PO4 gel electrolyte, and a PDMS-GO triboelectric film coated on the top surface of the device (this will be explained in more detail in the literature review section). This configuration would allow the full energy harvesting operation giving rise to high performance of the SCPC.

Objectives

1. To develop a low cost and flexible self-charging power cell by the integration of piezoelectric- triboelectric nanogenerator and reduced graphene oxide coated fabric supercapacitor with high self-charging performance.

2. To fabricate and optimize the PDMS-GO triboelectric nanogenerator to achieve high voltage and current outputs.

3. To fabricate PVDF-ZnO piezoelectric separator with high voltage and current outputs.

4. To investigate and optimize the capacitive performance of the flexible rGO coated fabric supercapacitors.

Scope of research

This project is going to fabricate a flexible SCPC which is an integration of piezoelectric-tribielectric nanogenerator. The ultimate goal of this work is to improve the self-charging performance the SCPC device by focusing on development of GO-based triboelectric nanogenerator and rGO-based supercapacitor. This will involve the fabrication of GO and PDMS nanocomposites to generate high current and voltage outputs, and the investigation of GO reduction condition to achieve the high quality rGO with excellent performance for supercapacitor electrodes. The GO and rGO characterization will be performed using Raman spectroscopy, Fourier transform infrared spectroscopy (FTIR). The morphology and structures of the device componenets will be examined using scanning electron microscopy SEM), X-ray diffraction, and transmission electron microscopy. The electrochemical properties will be measured using cyclic voltammetry (CV) and galvanostatic charge-discharge and electrochemical impedance spectroscopy (EIS).

Chapter 2

Literature review

Many SCPC devices have been developed in recent years. The fundamental mechanism of the SCPC was first introduced by Prof. Zhong Lin Wang's group which is explained in Fig. 1 [7]. The devices were the integration of a nanogenerator and a battery or a supercapacitor into one unit.

A typical SCPC has three main components: energy storage electrodes (cathode and anode), piezoelectric separator, and electrolyte. The self-charging mechanism in energy storage device is driven by the potential generated by mechanical deformation applied to the device through piezoelectric effect. The piezoelectric potential causes electrolyte ion to migrate to the electrode and the charging reactions to occur.

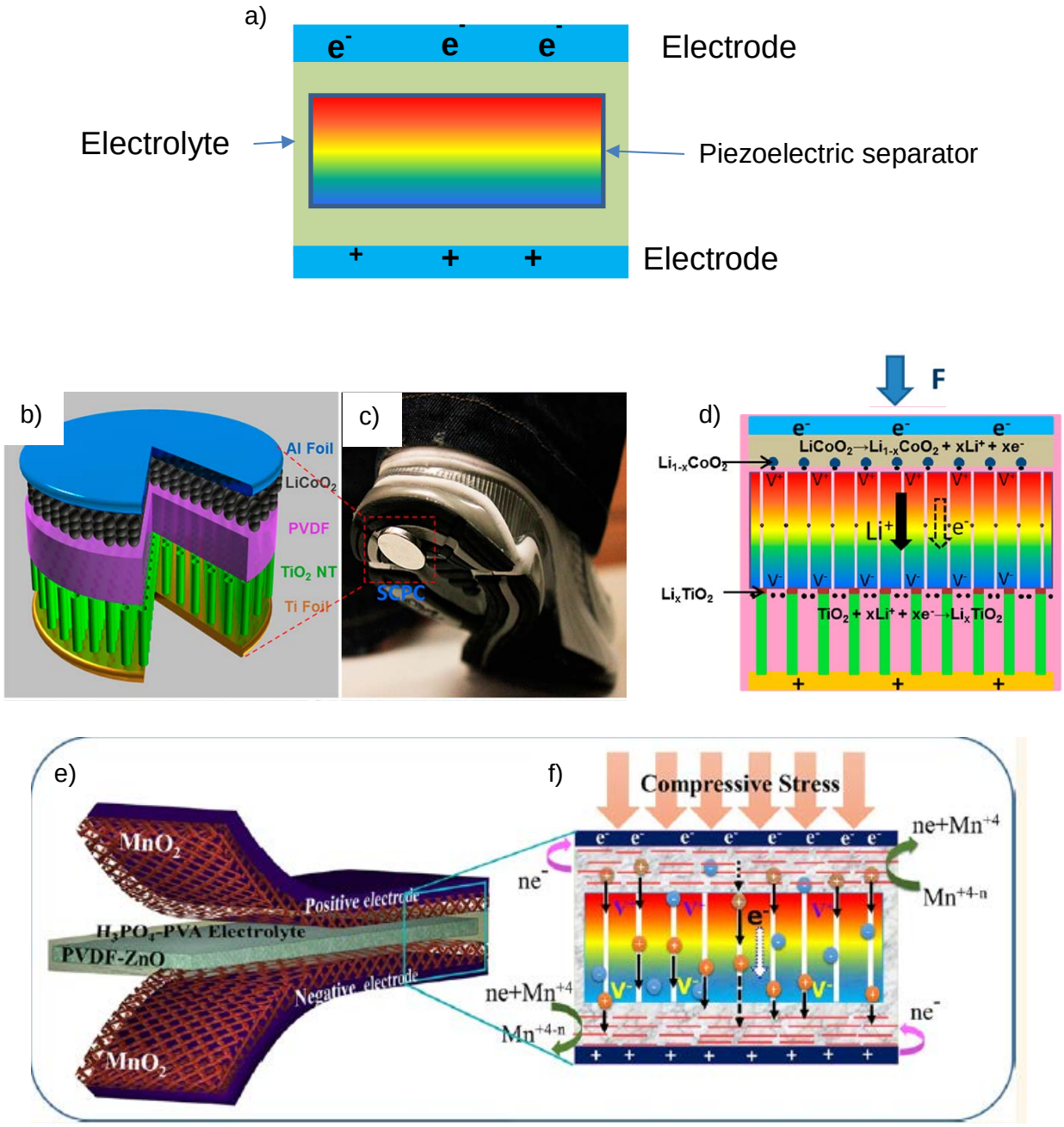

Figure 2.1 a) a typical SCPC device components, b), c) and d) a hybrid nanogerator - Li ion battery SCPC [7], e) and f) a hybrid nanogerator-supercapacitor SCPC [12].

Graphene, 2D zero band-gap semi metal, has been found to exhibit an exceptional electrical conductivity with high charge carrier mobility of 200,000 cm^2/V s at an electron density of 4 x 10^{-9} cm^{-2} which is six order of magnitude higher than that of copper [21]. The outstanding characteristics of graphene are that it has a large theoretical specific surface area (2630 m^2/g) and excellent mechanical flexibility [22]. Graphene would therefore an ideal material for fabricating flexible electrodes for supercapacitors. Graphene oxide (GO) is typically used as a precursor for producing graphene. The graphene produced by the chemical route is known as reduced graphene oxide (rGO); the reduction of graphene oxide to reduced graphene oxide (rGO) which is the most cost-effective and mass production of graphene nanostructures [23].

Recently, wearable electronic devices have gained a great deal of interests. Many graphene based textiles have been employed as supercapacitor electrodes including graphene based nanocomposites with some other capacitive materials coated onto various kinds of fabrics. Solution-exfoliated graphene nanosheets coated on porous textiles could yield specific capacitance of 63 Fg^{-1} and after forming graphene/MnO_2 nanocomposite the specific capacitance could go up to 315 Fg^{-1} [24]. A thermal annealed graphene coated cotton cloth composite fabric exhibited good electrical conductivity, outstanding flexibility, and high specific capacitance of 326.8 Fg^{-1} [25]. Graphene coated electronspun polyamide-66 nanofabric exhibited a specific capacitance of 280 Fg^{-1} [26]. Although capacitive performance of rGO is relatively inferior compared to MnO2, the simple cost effective fabrication that allows well deposition onto fabric would be beneficial for applying rGO as electrode material for supercapacitors.

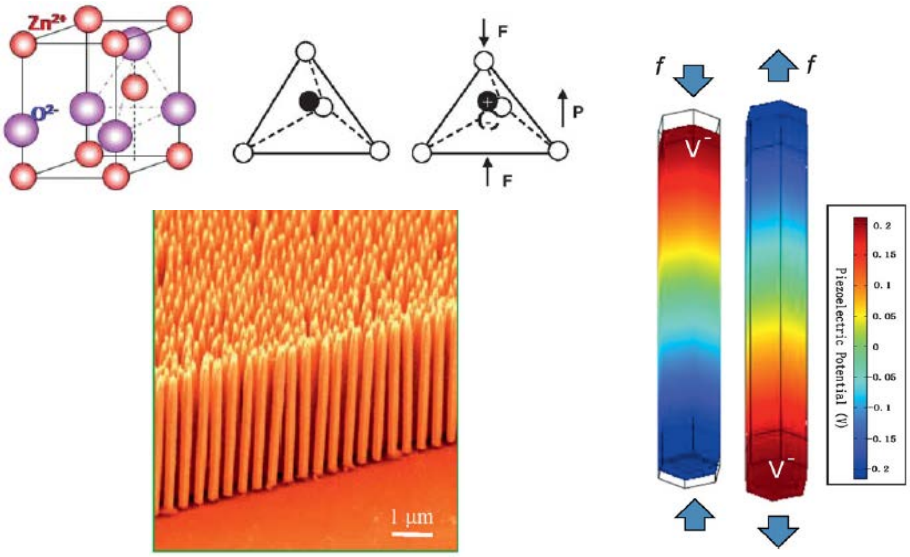

Figure 2.2 a) polarization created in Wurtzite structure of ZnO when strain is applied, b) vertically aligned ZnO nanowires [15].

ZnO-based piezoelectric nanogenerators are one of the most important candidates for developing self-powered nanotechnology [27, 28]. Piezoelectric effect is naturally generated when the strain is applied to a non-central symmetric wurtzite crystal structure of ZnO as shown in Figure 2. The dipole moment is generated when the a stress is applied at an apex of the tetrahedron in which the Zn^{2+} cations and O^{2-} anions are coordinated, which is caused by the displacement of the centers of the cations and anions. The polarizations from the entire structure produce a macroscopic potential or piezopotential along the strain direction in the structure. This generated piezopotential can drive a transient flow of electrons in an external load, which is the principle for the nanogenerator.

TENG can convert mechanical energy into electricity by using triboelectrification and electrostatic induction. Triboelectrification is a phenomenon that a material surface becomes electrically charged after it becomes into contact with another material. Insulating materials

usually generate a strong triboelectrification because they can capture the transferred charges and retain them for a long time at their surface. These captured charges serve as an electrostatic induction source for the electricity generation process of the TENG. This proposal is going to employ GO mixed with PDMS as a triboelectric layer on the basis of single electrode mode which is explained in the working mechanism below. The reason for mixing GO and PDMS is to prevent the GO intermixing with rGO in another side of the electrodes. The SCPC device components and its working mechanism are described in Figure 3 and 4, respectively.

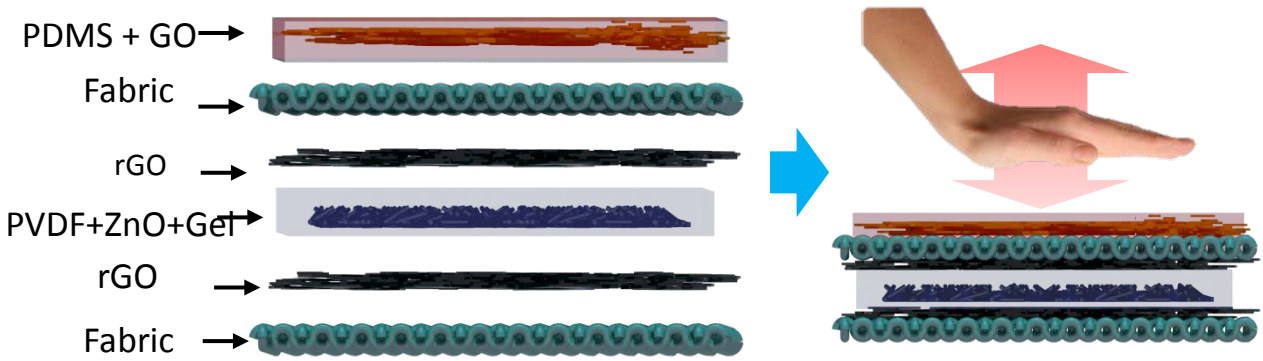

Figure 2.3 The flexible SCPC by integration of piezoelectric- triboelectric nanogenerator and reduced graphene oxide coated fabric supercapacitor.

Working mechanism

1. At the initial there is no force applied to the device, the device is in discharge state (Fig. 2.4a)).

2. As the compressive stress is applied to the device by human palm on the top side of the device, this cause the polarization of the PVDF-ZnO separator by piezoelectric effect. The polarization of ions generates a potential difference across the thickness of the separator (Fig. 2.4b)). A negative and positive piezoelectric potential is generated at the top and bottom of the device respectively. This potential drives the electrolyte ions (PVA/H_3PO_4) toward the positive and negative electrodes to the charge state (Fig. 2.4c)). Simultaneously, human palm and PDMS+GO layer contact with each other, resulting in the charge transfer between them. Electrons are injected from the skin to the PDMS+GO because PDMS+GO layer is more tribolelectrically negative than skin, which is the contact electrification process.

3. When human palm move up away from the device (Fig. 2.4d)), there is no compressive stress and hence piezoelectric potential is no longer available to drive the ions to the electrodes. However, the separation of the human palm and PDMS+GO cause charge unbalance. The negative charge on the surface of the PDMS+GO can induce positive charge on the carbon fiber electrode, driving the free electron to flow from the carbon fiber electrode to the electrolyte. These free electrons can retain the cations (H^+) through coulomb interaction at the top electrode of the device whereas anions are stored at the bottom electrode.

4. As the human palm moves toward the PDMS+GO again (Fig. 2.4b)), the free electrons flow back to the carbon fiber until they fully contact to each other again. The stress applied by human palm generated piezoelectric potential again. With continuing applied force to the device, the charging cycle is repeated.

5. These synergistic processes of piezoelectric and triboelectric would significantly enhance the self-charging performance of the SCPC device by a conversion of mechanical energy directly into electrochemical energy.

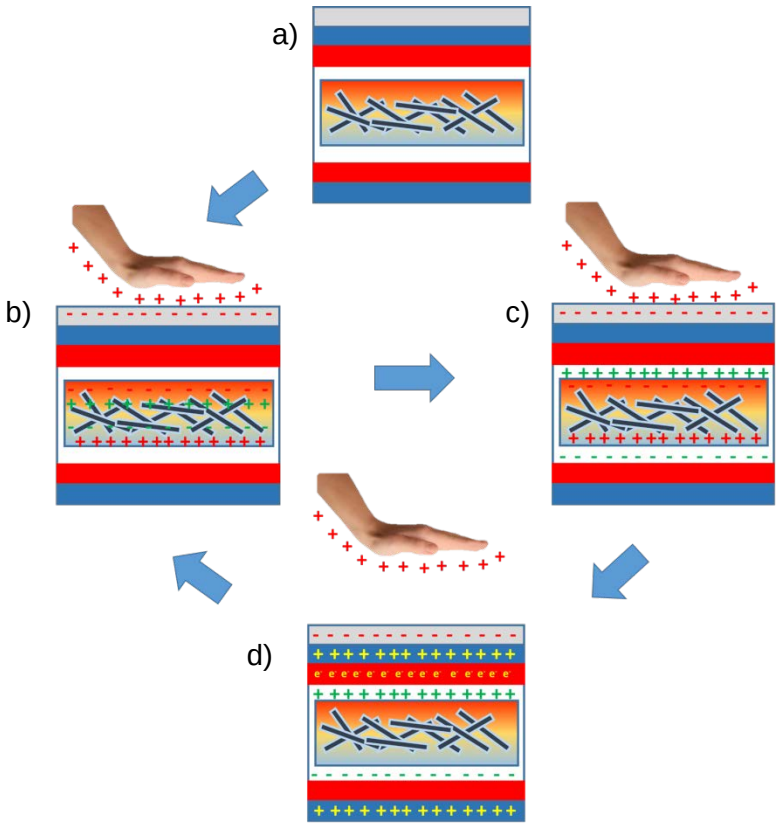

Figure 2.4 working mechanism of the flexible SCPC by integration of piezoelectric-triboelectric nanogenerator and reduced graphene oxide coated fabric supercapacitor

Chapter 3

Experiment

In this work, PDMS and GO triboelectric nanocomposite material was prepared and test for the nanogenerator performance. Then it was used as a triboelectric component for the self-charging power cell.

3.1 *PDMS-GO composite for triboelectric materials*

A PDMS solution (Sylgard 184, Dow Corning) containing both the elastomer and curing agent in a mass ratio of 10:1 was prepared for the flat, pristine PDMS film. For the PDMS@GO composite film, a GO solution with various concentrations (2, 4, 6, and 8 mg/mL) was mixed with a PDMS elastomer solution in a volume ratio of 1:5 through magnetic stirring for 30 min. For simplicity, these samples are hereafter referred to as PDMS@GO-2, PDMS@GO-4, PDMS@GO-6, and PDMS@GO-8, respectively. For the porous PDMS@GO@SDS films, the SDS surfactant was dissolved in the 4 mg/mL GO suspension at concentrations of 0.1, 0.2, 0.3, and 0.4 M before mixing with the elastomer solution, and the corresponding samples are hereafter referred to as PDMS@GO@SDS-0.1, PDMS@GO@SDS-0.2, PDMS@GO@SDS-0.3, and PDMS@GO@SDS-0.4, respectively. Next, the curing agent was added to each suspension, and stirring was resumed for 15 min to obtain a uniformly dispersed solution. The negative electrodes of the TENGs were spin-coated onto a 2 × 2.5 cm Au-coated glass substrate whose surface was undergone pre-treatment step to promote the adhesion by immerse in 5 mM (3-mercaptopropyl)trimethoxysilane (MPTMS) solution for 30 min.[29] The PDMS composite films were then cured at 80 °C for 2 h, and water was removed at 150 °C for 2 h using a hot plate. The fabrication process for PDMS@GO is illustrated in Fig. 3.1.

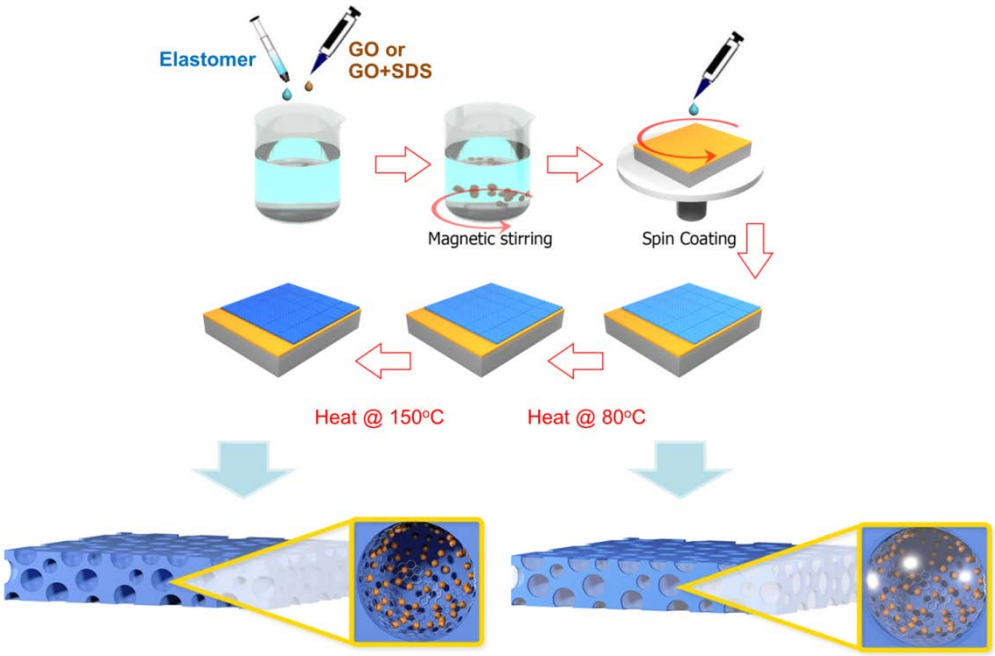

Figure 3.1 The schematic illustrates the fabrication of PDMS@GO films as negative triboelectric materials.

3.2 Preparation of PVDF-ZnO piezoelectric layer as a separator

ZnO nanowires are purchased from *Sigma Aldrich*. PVDF-ZnO layer is going to prepared by mixing PVDF in acetone/DMF solvent with the volume ratio of 6:4 and the prepared ZnO nanowire. The ratio of PVDF to ZnO nanowire to get the optimum performance will be investigated. Then the mixture will be dried at 50^{o}C for 4 hours.

3.3 Preparation of rGO electrode for supercapacitor

3.3.1 GO synthesis

Graphene oxide is synthesized by using modified Hummers method which can be explained briefly as follows. The mixture of graphite powder and $NaNO_3$ are firstly prepared, then 95%

H_2SO_4 is added to the mixture, $KMnO_4$ is slowly added to the solution. Then the mixture is stirred at room temperature for 2 hours. Then DI water is added and the diluted mixture is stirred at 98 ^oC for 12 h. Then H_2O_2 (30%) is added to the prepared solution. Finally, the mixture is purified by washing and rinsing with 5% HCl solution and demonized water for several times. After centrifuged and dried in vacuum, graphene oxide will be obtained in the form of black powder. The produced graphene oxide will be characterized by UV-VIS spectroscopy, Raman spectroscopy, Fourier transform infrared spectroscopy (FTIR). In this research, graphene oxide will be provided by Prof. Dae Joon Kang.

3.3.2 rGO coated fabric

The carbon fabric is cleaned in ethanol, acetone, and deionized water in a sonicating bath. The GO power is dispersed in DI water with a concentration of 2 mg/ml and ultrasonicated for 2 hours to form a stable suspension. The cleaned carbon fabric is coated by GO solution by repeated dip-coating at 60 ^oC for 30 min for 5 times. Then GO-coated fabric is thermally reduced to for rGO-coated fabric at 160^oC in Ar for 2 hours.

3.3.3 GO+PDMS triboelectric

One side of one of the two rGO-coated fabric electrodes of the supercapacitor is coated by the GO+PDMS. The reason for mixing GO with PDMS is for preventing GO disperse through the opposite side of the fabric which is previously coated by rGO.

PDMS prepolymer made by mixing base silicone gel with a curing agent in a 10:1 weight ratio is dissolved in dichloromethane to obtain homogeneous solution. Then GO powder is mixed into the solution and sonicated for 2 hours. The mixture is coated on to one side of dried at room temperature for 2 h and cured at 90 ^oC for 2 h. Then the GO+PDMS triboelectric layer is obtained. The ratio of the GO: PDMS will be studied and optimize to achieve the optimum condition.

3.4 *SCPC cell assemble*

The SCPC is assembled by two rGO- coated fabric electrodes with the rGO-coated side facing toward each other while the GO+PDMS side is on the top surface of the device. PVA/H_3PO_4 gel electrolyte and PVDF-ZnO separator (section 1) in the middle are then insert between the two electrodes. Then the assembled SCPC is dried at room temperature for 12 h. Then the flexible SCPC by integration of piezoelectric-triboelectric nanogenerator and supercapacitor can be finally achieved.

The performance of each functional part; PVDF-ZnO piezoelectric, GO+PDMS triboelectric and rGO supercapacitor will be investigated.

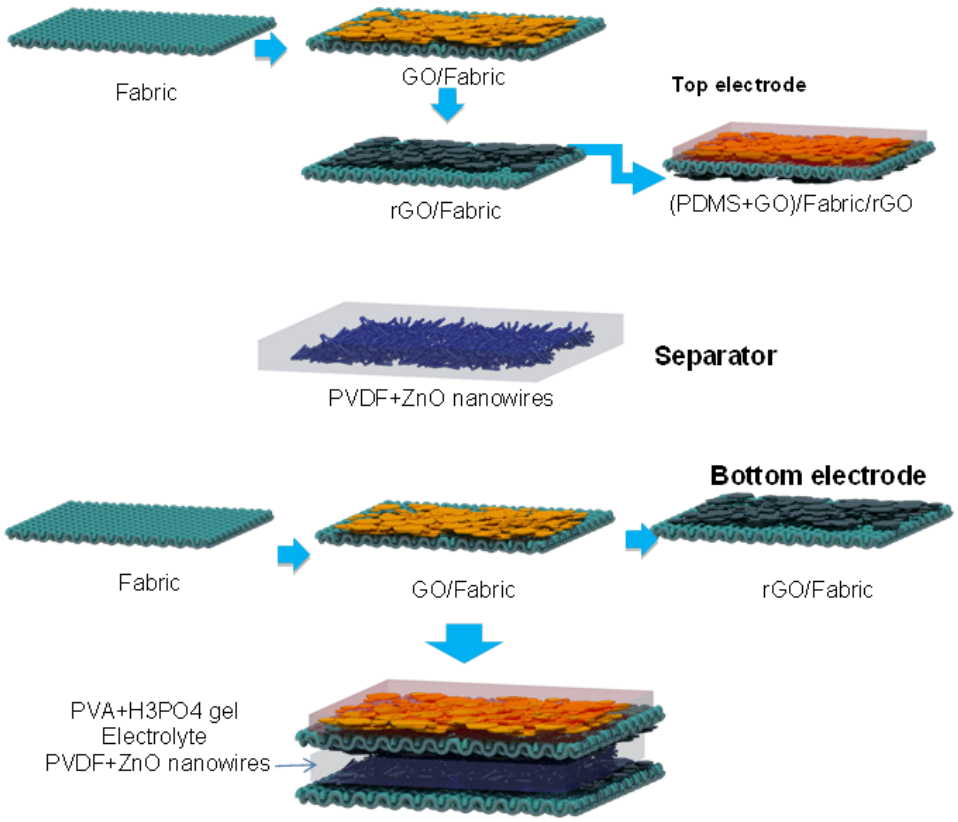

Figure 3.2 Device fabrication

3.5 Device performance

3.5.1 Output voltage and current of nanogenerators

Piezoelectric and triboelectric nanogenerators and SCPC devices are examined using the pressing and bending test system (Teraleader). The electric characteristics of the nanogenerator devices are measured using oscilloscope (LeCroy WavePro 715Zi) and a low-noise current preamplifier (Stanford Research System SR570).

3.5.2 Supercapacitor characterization and measurement

Cyclic voltammetry (CV), galvanostatic charge-discharge and impedance measurement are performed using CHI-660 B electrochemical station (CH Instrument Inc, TX, USA). The cyclic voltammograms, specific capacitance, energy density, power density, stability of supercapacitor and the self-charging performance of SCPC are characterized.

3.6 *The structure characterization*

The structure of the samples is characterized by X-ray diffraction and Raman spectroscopy techniques. The morphology of the samples is examined using FE-SEM.

Chapter 4

Results and discussion

First, the effects of GO concentration on the morphology of the PDMS@GO composite films and their voltage and current outputs were investigated. Fig. 4.1a shows SEM images of the PDMS@GO with 2–8 mg/mL GO. In contrast with flat PDMS, the PDMS@GO films feature porous structures due to the formation of bubbles by the indissoluble GO in the PDMS. Although the porous structures show no significant differences among the various GO concentrations, the pore density increases with the GO concentration. The output performance of the various PDMS@GO films exhibits a notably similar trend, as shown in Fig. 4.1b. As the GO concentration increases, the output voltage and current reach their maximum values of 215 V and 6 μA/cm^2, respectively, with the 4 mg/mL GO sample. The outputs then decrease with the increased GO concentrations of 6 and 8 mg/mL.

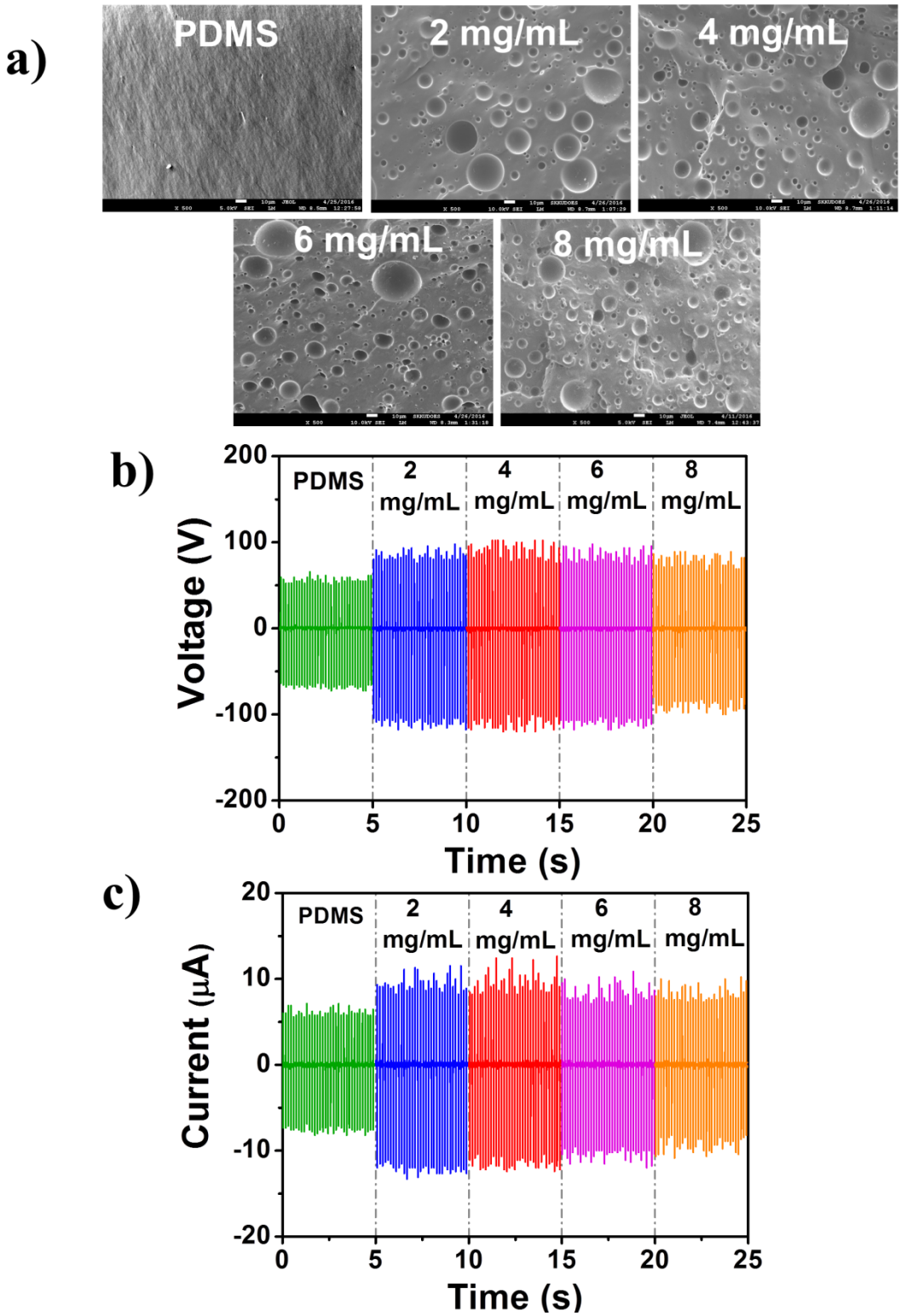

Fig. 4.1. (a) SEM images and the (b) voltage and (c) current output of PDMS and PDMS@GO films with various GO concentrations.

To elucidate the lower performance at high GO concentrations in the PDMS@GO composite films, Raman spectroscopy analysis was performed, as presented in Fig. 4.2a. The

characteristic Raman spectrum of PDMS is consistent with that in the relevant literature. The two peaks at 1345 and 1595 cm^{-1} are assigned to the disorder-induced D bands and in-plane C–C stretching G bands of GO, respectively. The Raman spectra of the composite films contain the superimposed spectra of both PDMS and GO with no additional peaks, suggesting that no chemical interaction occurred between the two components. The Raman spectra of two pristine GO films heated at 80^{o}C and 150^{o}C were acquired to probe the transformation of GO during the fabrication process. The I_D/I_G ratios which can be used as the measure of defect/disorder density in GO were found to slightly increase from ~1.0 to ~1.1 in the 80 ^{o}C and 150 ^{o}C heated GO (representing the composite films at all GO concentration) respectively (supplementary Fig. S1).[30-32] These numbers are still lower than those determined in some previous studies [33, 34] suggesting that GO was partially reduced forming rGO but the degree of reduction was relatively low. The increase in the D peak intensity after the 150 ^{o}C heating indicates that more oxygen functional groups were introduced into carbon chains which could be surface hydroxyl and/or epoxy groups from vaporized water.[35]

To support the Raman data, a C 1s XPS spectrum was acquired from the best-performing PDMS@GO-4 composite film (the 4 mg/mL GO film), as presented in Fig. 4.2b. The deconvoluted C 1s XPS spectrum reveals four C components in the composite. The C–C and C–OH/C-O components at ~285 and ~286 eV are from covalent carbon bonds and hydroxyl/epoxy groups, respectively.[35, 36] Two other C–Si components at ~283.5 and 284.5 eV are obtained from the bonding between the C and Si atoms in the substrate and in the PDMS molecules, respectively. The intensity ratio of the C–C and C–O components ($I_{C–C}/I_{C–O}$) in the XPS spectrum verifies the reduction of GO, which forms rGO in the composite.

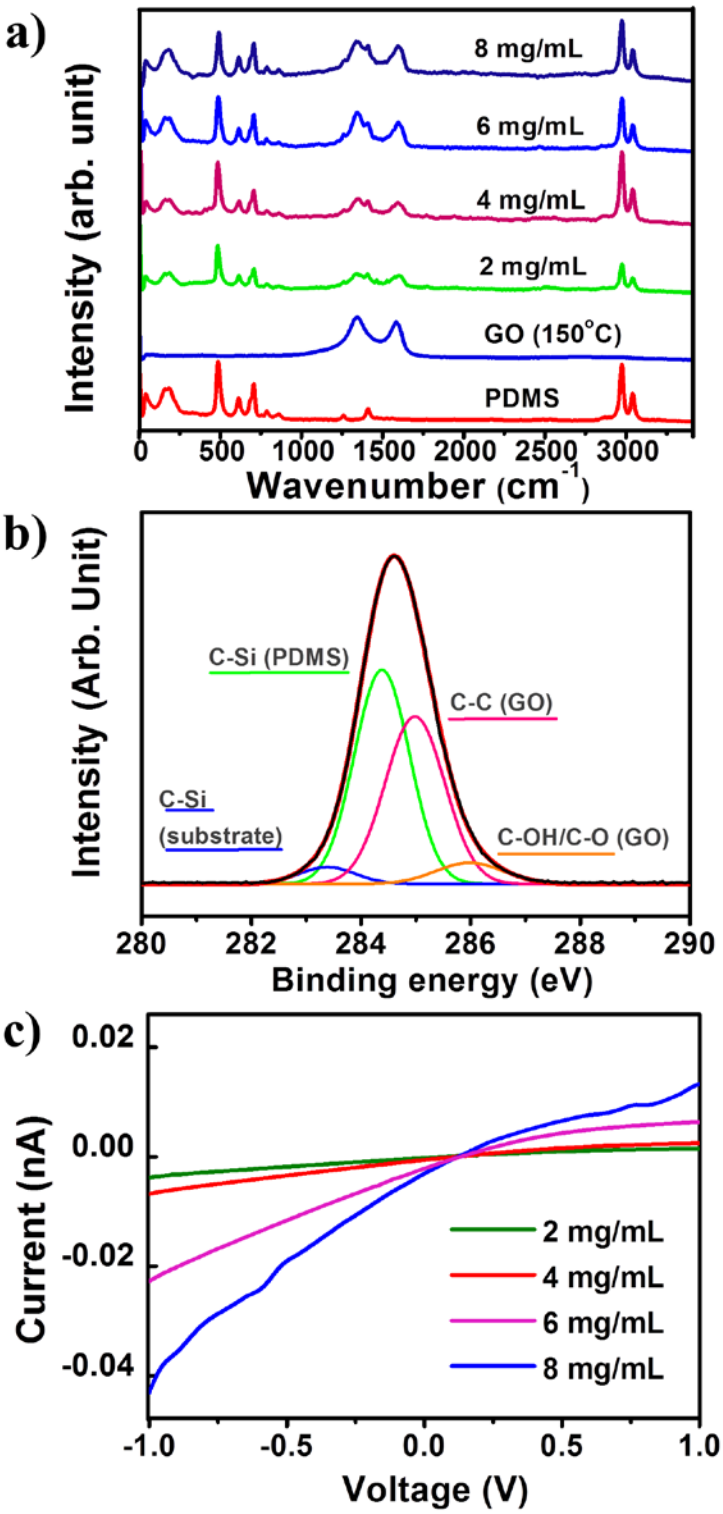

Figure 4.2 (a) Raman spectra of the PDMS and PDMS@GO films with various GO concentrations, (b) C 1s X-ray photoelectron spectra of the 4 mg/mL PDMS@GO composite film, and (c) I–V measurements of the composite films.

The fabrication steps and a proposed model of the porous PDMS@GO composite are shown in Fig.4.3. In the PDMS@GO composite film, the aqueous GO suspension is not dissolved in the PDMS prepolymer; thus, small droplets of GO solution disperse inside the PDMS matrix under magnetic stirring. Next, annealing is performed i) at 80 °C to cure the PDMS film and ii) at 150 °C to evaporate the water trapped inside the droplets. Annealing at 150 °C in the ambient atmosphere is likely to have synergistic effects: removing the confined water bubbles, thereby producing the porous film, leaving behind more negative surface functional groups and partially reducing the GO. The rGO clusters in the insulating the PDMS matrix act as charge trapping sites that can induce a capacitance effect, which has also been observed in previous studies[37-39]. These synergistic effects account for the improved output performance of the PDMS@GO TENG.

However, the decreased output performance at higher GO concentration can be ascribed to the electrical percolation of the rGO network in the PDMS matrix,[40, 41] as evidenced by the increasing conductivity shown in the current–voltage (I–V) measurements in Fig. 4.2c. The resistances of all the composite films were relatively high (10^9 Ω) and decreased with the increasing GO concentration. The higher GO precursor concentrations resulted in the connection of the conductive rGO network, as shown in the SEM images of the dense porous structure in the fabricated PDMS@GO-6 and PDMS@GO-8 films in Fig. 4.1a. The electrical percolation directly affects the output performance of the composite TENGs because of the dissipation of electrified charges, thus resulting in a decrease in the potential and current output.

The PDMS@GO films exhibit relatively wide size distributions of bubbles or pores, which range in diameter from a few micrometres to a few tens of micrometres. To optimize the uniformity of the porous structures, to homogeneously disperse the GO clusters in the PDMS

matrix, and to enhance the specific contact area, an SDS surfactant was added to the mixture of PDMS and GO. Moreover, the anionic head groups of the SDS molecules were expected to further intensify the negative charges in the composite films.

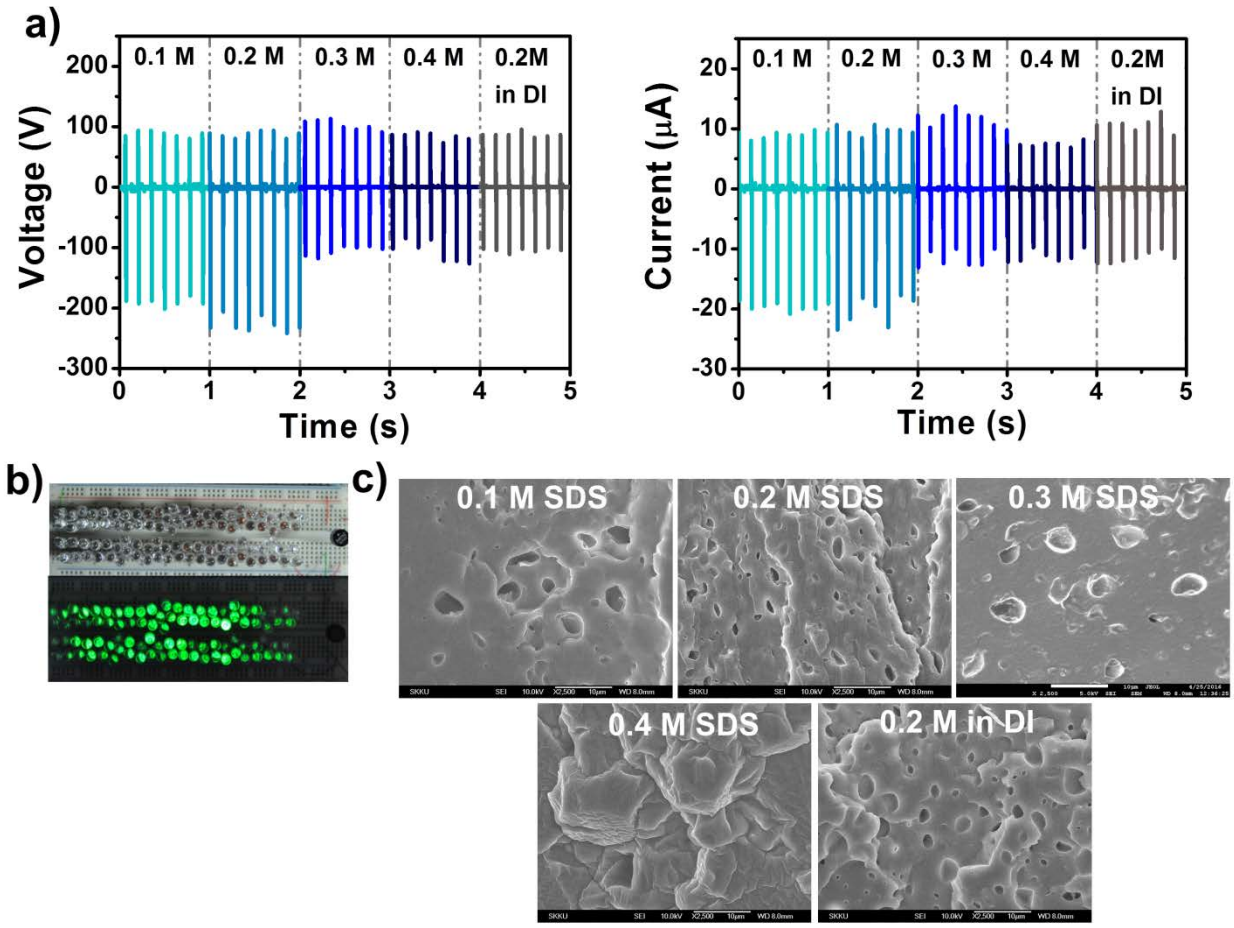

Figure 4.3 (a) Output voltage and current of the PDMS@GO@SDS composite TENG with various SDS concentrations; (b) 90 LEDs can be illuminated using 0.2 M SDS PDMS@GO@SDS TENG, and (c) the SEM images of the PDMS@GO@SDS composite films with various SDS concentrations.

Fig. 4.3a presents the effect of the SDS concentration on the output performance of the PDMS@GO@SDS TENGs. The highest output voltage and current of up to 330 V and 8

μA/cm^2, respectively, were achieved for PDMS@GO@SDS with 0.2 M SDS. This can power 90 green light emitting diodes (LEDs), as shown in Fig. 4.3b and the video S2 in the supporting information. The achieved output performance was approximately 1.5 times greater than that of the PDMS@GO-4 TENG. At high SDS concentrations, the output performance deteriorated to almost the same output as that of the PDMS@GO without SDS. The SEM images shown in Fig. 4.3c reveal the remarkable changes in morphology among the PDMS@GO@SDS samples with various SDS concentrations.

When the SDS surfactant is initially added to the GO solution prior to being mixed with the PDMS prepolymer, the hydrophilic negatively charged head groups of the SDS molecules are electrostatically repelled from the negatively charged oxygen-containing functional groups on the GO surface. Thus, SDS molecules are not adsorbed onto the GO but form micelles in the solution.[42] In contrast, SDS alkyl chains have been demonstrated to adsorb on rGO surfaces, and their absorption behaviour was found to depend on the SDS concentration and the degree of GO reduction.[43, 44] In this study, the SDS concentration is relatively higher than the typical critical surface aggregation concentration reported in previous studies.[43, 44] The SDS molecules are expected to form hemicylindrical and/or hemispherical surface micelles[45] and micelles in bulk solution. If the SDS concentration is extremely high (0.4 M), the morphology of the composite becomes granular and discontinuous, thus deteriorating the output performance of the TENGs.

Fig. 4.4 shows the SEM-EDX mapping of S $K\alpha_1$, C $K\alpha_{1,2}$, and Si $K\alpha_1$ in the PDMS@GO@SDS. Sulfur was detected across the sample with some porosity, suggesting the uniform dispersion of the SDS molecules in the composite and the micelle formation in the precursor solution. However, the yellow circles and arrows in Fig. 4.4a) and 4.4b) indicate areas of high sulfur density, suggesting the presence of rGO with adsorbed SDS

molecules located close to the holes. This could indicate the presence of rGO on the sidewalls of the pores.

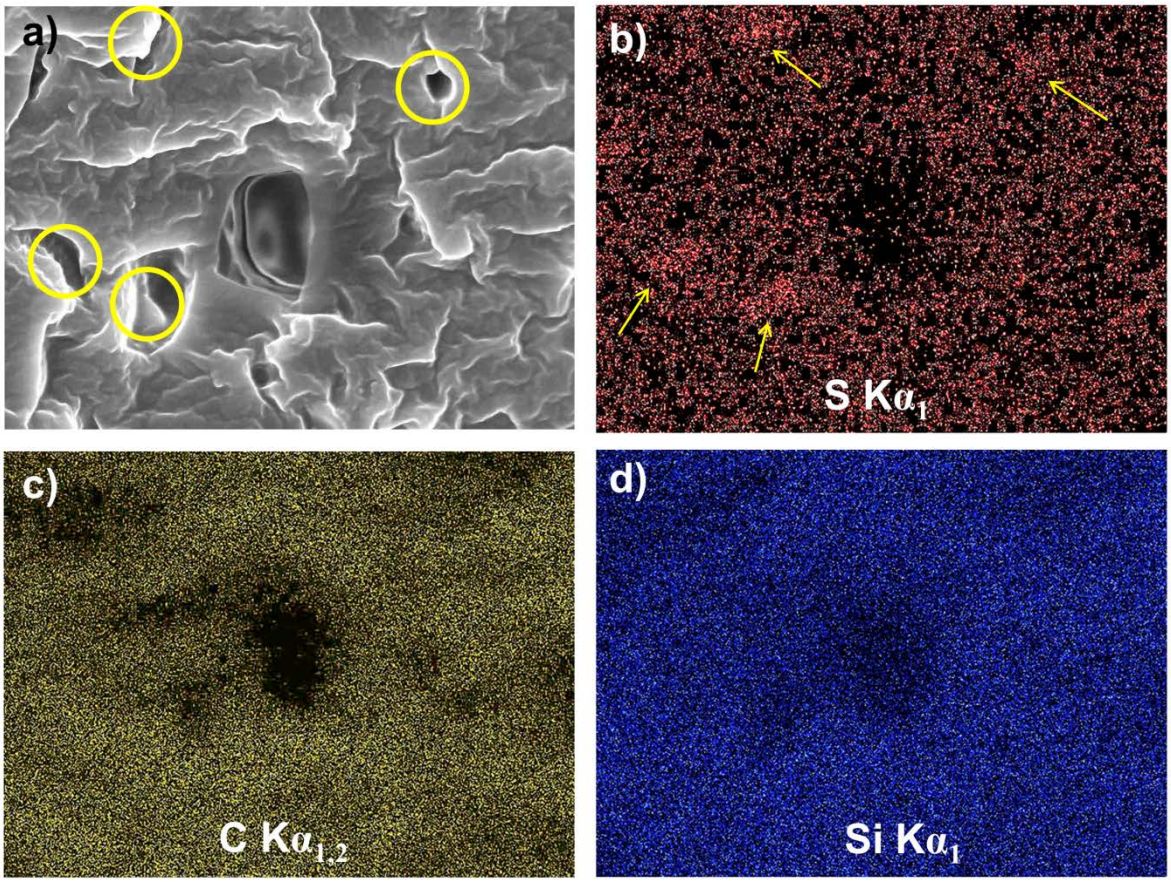

Figure 4.4 (a) SEM image and SEM-EDX mappings of (b) S $K\alpha_1$, (c) C $K\alpha_{1,2}$, and (d) Si $K\alpha_1$ in the PDMS@GO@SDS film with 0.2 M SDS concentration.

The working principle of the fabricated PDMS@GO@SDS TENG under a single-electrode mode is presented in the schematic diagram in Fig. 4.5, using a polyethylene naphthalate (PEN) film with indium tin oxide (ITO) deposited on the top as a moving electrode with the PEN side facing the PDMS@GO@SDS film, which was spin-coated on an Au-coated glass substrate. In the initial state, the two film surfaces are not in contact, no charge transfer occurs, and hence, no electric potential exists. When the two materials are brought into

contact, electrons transfer between the PEN and PDMS films upon electrification, producing positive and negative charges at the surfaces of the PEN and PDMS@GO@SDS films, respectively, as a result of the chemical potential difference.

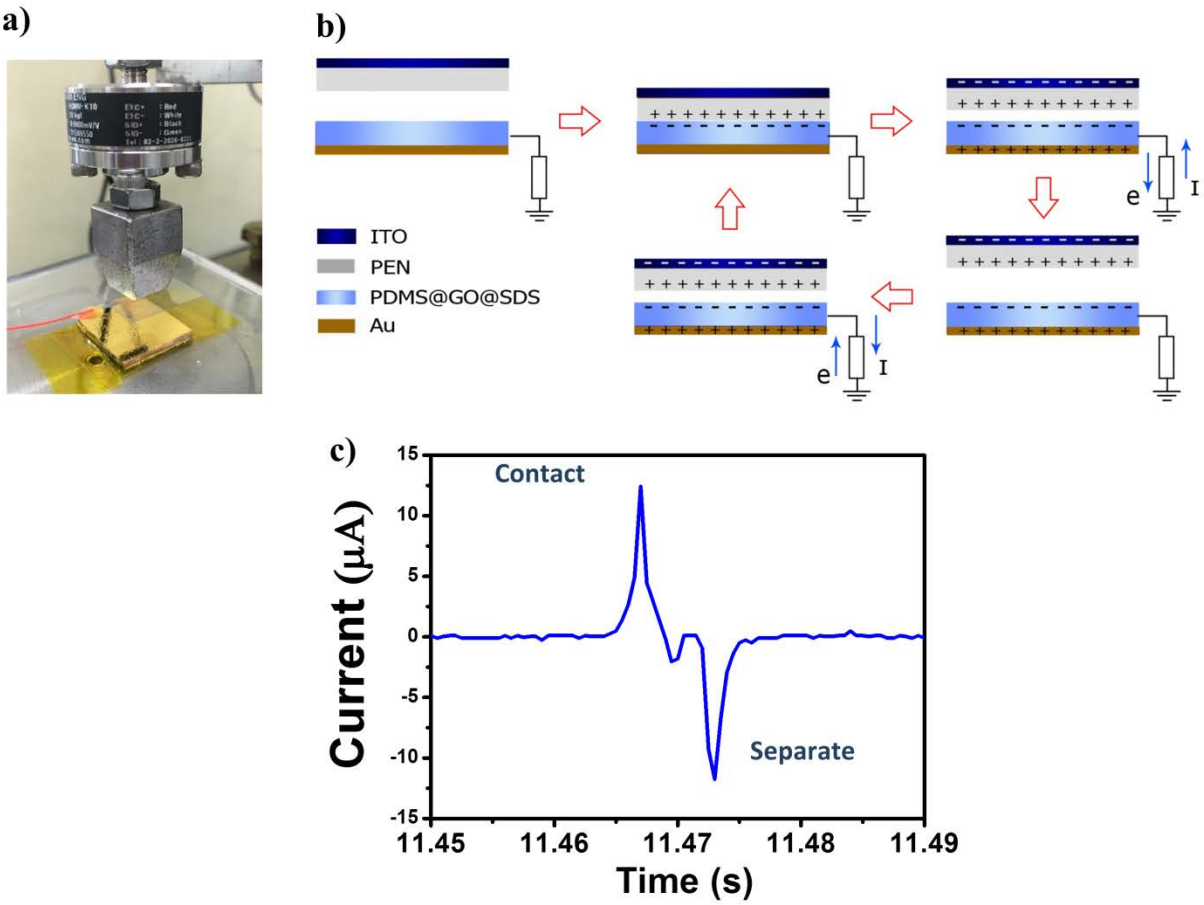

Figure 4.5 (a) Output measurement, (b) the schematic presentation of working principle of the fabricated TENG in the single-electrode mode, and (c) the measured current output signal.

When the two surfaces are separated, the electric potential created by the triboelectric charges on the surfaces drives free electrons in the bottom Au electrode to flow to the ground to neutralize the negative charges on the composite film, leaving a positively charged Au electrode and generating a negative voltage signal. Simultaneously, the positive charges on

the PEN surface can induce free electrons in the ITO top layer to reside at the interface without tunnelling through the PEN film. In the single-electrode operation mode, the ITO is not connected to the bottom Au electrode, and consequently, this configuration provides electrostatic attraction which can confine positive surface charges on the PEN throughout the electrification process; otherwise, some of the electrified charges can dissipate into the atmosphere due to water molecules in the air.[46] When the two surfaces are brought back into contact again, the potential experienced by the free electrons in the bottom electrode decreases, and they thus flow back from the ground to neutralize the earlier positively charged Au electrode, producing a positive voltage signal.

In this study, the output performance was significantly augmented by increasing the charge density. Considering a simple contact mode operation, the output voltage (V) and the voltage at the open circuit (V_{oc}); no transferred charge, are given by Equations (1) and (2).[47]

$$V = \frac{(\sigma_0 - \Delta\sigma) \cdot x(t)}{\varepsilon_0} - \frac{\Delta\sigma \cdot d}{\varepsilon_0 \varepsilon_r} \quad (1)$$

$$V_{oc} = \frac{\sigma_0 \cdot x(t)}{\varepsilon_0} \quad (2)$$

where σ_0, $\Delta\sigma$, $x(t)$, ε_0, d, and S represent the triboelectric charge density on the film surface, transferred charge density on the electrode, a distance between the surfaces of two triboelectric materials, vacuum permittivity, triboelectric film thickness, and the film surface area, respectively.

The maximum voltage V_{oc} that can be achieved at the maximum distance between the two triboelectric material surfaces is governed by the triboelectric charge density, σ_0. In this study, the superior output performance of the fabricated TENG is attributed to the synergetic contributions of the PDMS@GO@SDS composite film. First, the oxygen functional groups

in the rGO and the anionic head groups of the SDS surfactant molecules provide abundant negative charges. Second, the improved dispersion of rGO in the PDMS results in the increased contact surface area of the sub-10-μm porous structure.

The transfer charges Δσ were obtained from the integration of the output current plots ($\Delta\sigma = I\Delta t$) with the use of 10 MΩ input load resistance and the measured Δσ values of all samples are presented in Table 1. The charges transfer from ground to the electrode during contact state and from the electrode to ground during separation state is illustrated in Fig. 4.5b) and c). The transfer charge was the highest at the PDMS with 4 mg/mL GO and 0.1M SDS which corresponded to its highest output current density.

To further optimize the performance of the composite TENG, the effects of the film thickness, operation force, and contact–separation frequency on the TENG performance were investigated. In addition, the triboelectric charge density σ is dependent on the capacitance *C* of the TENG, relative dielectric constant (ε_r), surface area (*S*) and thickness of the dielectric film (*d*) as described by Equations (3) and (4).

$$\sigma_0 = \frac{C\Delta V}{S} = \frac{\varepsilon_0 \varepsilon_r \Delta V}{d} \qquad (3)$$

or

$$C = \frac{\varepsilon_0 \varepsilon_r S}{d} \qquad (4)$$

According to these equations, a thin film is expected to exhibit a high performance. However, the optimum film thickness that can produce the highest output performance was determined to be 5 μm, as shown in Fig. 4.6a and 4.6b. The thinner film degraded the TENG performance because of the small number of charges. The output performance of the PDMS@GO@SDS TENG gradually increases with the applied force from 1 to 10 N at an operation frequency of 7 Hz with a 5 μm thick film (Fig.4.6c). The output voltage and current

both increase gradually and become almost stable after 6 N. This could be because at 6N applied force provides the maximum frictional contact of the surface and inner structure of the porous composite film.

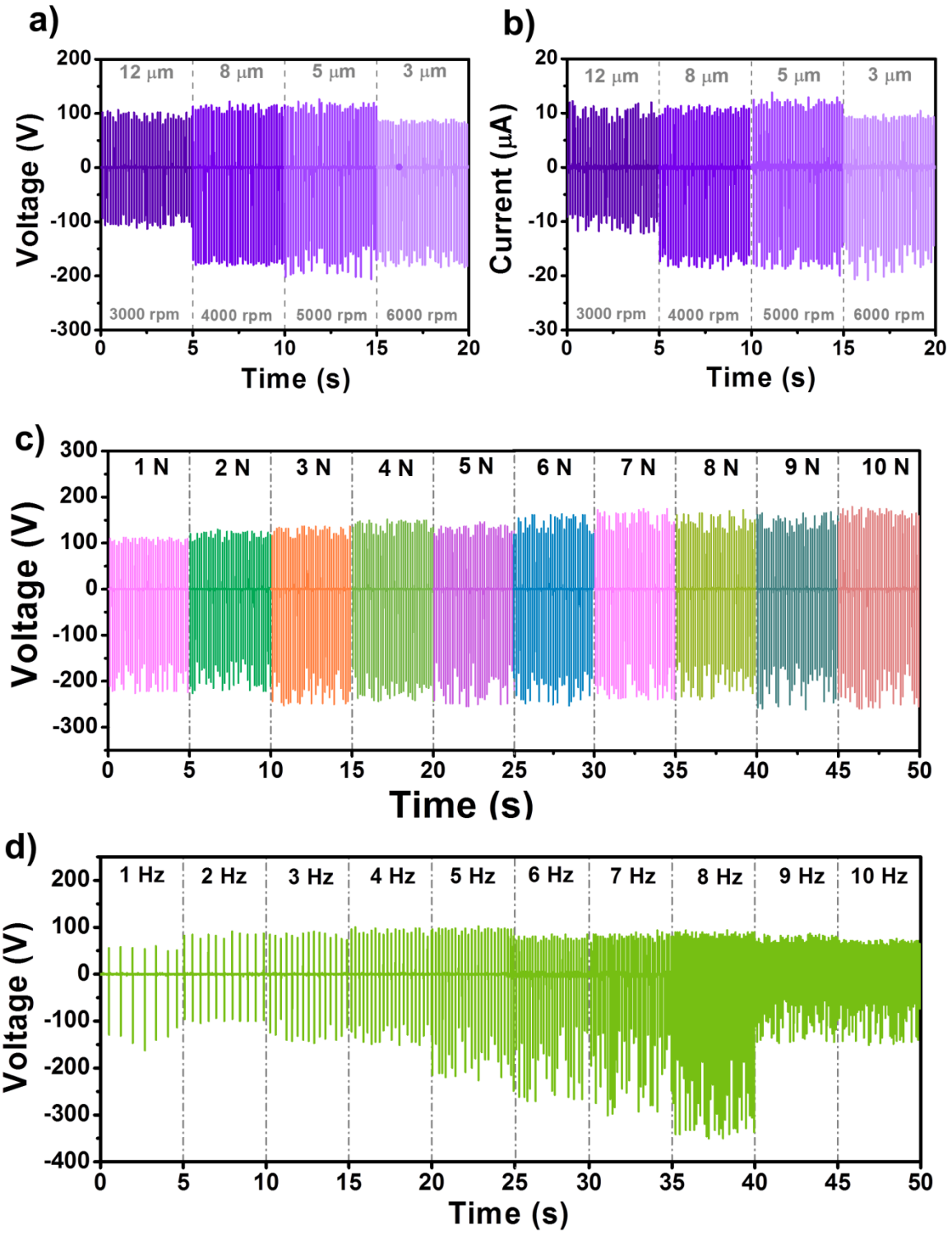

Figure 4.6 Dependence of the PDMS@GO@SDS TENG output performance on the (a) and (b) film thickness, (c) force, and (d) contact–separation frequency.

Material	**Synthesis condition**	**Frequency (Hz)**	V_{oc} **(V)**	**Current (peak to peak) (μA)**	**Transfer Charge Δσ (nC/cm^2)**	
					Contact	**Separate**
PDMS	Flat	5	125	14	11.3	12.8
PDMS@GO	GO 2mg/mL	5	204	24	15.6	18.0
	GO 4mg/mL	5	218	25	16.6	17.9
	GO 6mg/mL	5	204	20	16.1	16.6
	GO 8mg/mL	5	173	19	12.7	14.3
PDMS@GO@SDS [GO 4mg/mL]	SDS 0.1 M	5	278	30	16.2	22.5
	SDS 0.2 M	5	331	33	16.3	23.8
	SDS 0.3 M	5	226	23	16.4	23.2
	SDS 0.4 M	5	213	19	12.0	16.8
PDMS@GO@SDS [GO 4mg/mL] [SDS 0.2 M]		1	200	16	11.5	15.7
		2	188	21	16.5	22.3
		3	230	24	17.2	23.0
		4	246	25	17.3	22.2
		5	317	35	17.2	23.5
		6	342	37	15.6	22.3
		7	377	44	15.3	23.2
		8	412	45	14.4	21.0
		9	215	26	12.2	15.4
		10	213	26	10.8	14.6

Table 1 Maximum voltage and current out puts extract from output signals in Fig. 1, 4 and 7 and their transfer charge densities.

The frequency dependence was also investigated with a 5 μm thick film and a constant force of 6 N; the output performance increases with the operation frequency up to 8 Hz, when the maximum output voltage and current of up to 438 V and 11 μA/cm^2 are achieved, respectively, as shown in Fig. 4.6d and the video S3 in the supporting information. This dependence could be due to the accumulation of surface charges (σ_0) on the composite material surface that could not be completely neutralized at a high frequency, which can be seen from the reduced transfer charges starting at the frequency of 6 Hz in Table 1. However, at higher operation frequencies of 9 and 10 Hz, the performance dramatically dropped, which could be attributed to the extremely high number of accumulated charges σ_0, which can screen the potential because of the free electrons transferring between the Au electrode and the ground, thereby decreasing the generated current and voltage.

The effective power density of the TENG can be estimated from the formula $P=V^2/RA$, where V is the output voltage, R is the load resistance, and A is effective size of the TENG. For our output measurement, the input resistance of the oscilloscope is 10 MΩ, the maximum output power density of the PDMS@GO@SDS is then ~4.8 mW/cm^2.

Table 2 summarizes the output performance under a compressive force of 1 N at 7 Hz. The addition of only GO or SDS demonstrated relatively similar performance; however, when both GO and SDS were mixed into the PDMS to form a PDMS@GO@SDS composite, the output performance greatly improved to almost three times that of the flat PDMS film.

Samples	Voltage (V)	Current (μA)
PDMS	131	14
PDMS@GO	215	25
PDMS@GO@SDS	330	32
PDMS@SDS (water)	198	22

Table 2. Output performance summary at pressing operation under 1 N of force at 7 Hz.

Chapter 5

Conclusion

A PDMS@rGO@SDS composite film was successfully developed as a high-performance negative triboelectric material. Under the optimum operating conditions, an output performance three times greater than that of a flat PDMS film was achieved, namely, a maximum output voltage and current of 438 V and 11 μA/cm^2, respectively. The negative charge density was intensified by the SDS surfactant and rGO, and the latter also provided enhanced charge trapping. These improvements, in combination with the high contact area of the porous structure, account for the superior output performance of the PDMS@rGO@SDS composite film. This novel approach is conducive to the facile, scalable production of high-performance TENGs.

References

1. Hinchet, R., W. Seung, and S.-W. Kim, *Recent Progress on Flexible Triboelectric Nanogenerators for SelfPowered Electronics.* ChemSusChem, 2015. 8(14): p. 2327-2344.
2. Ha, M., et al., *Triboelectric Generators and Sensors for Self-Powered Wearable Electronics.* ACS Nano, 2015. 9(4): p. 3421-3427.
3. Wang, Z.L., *Triboelectric Nanogenerators as New Energy Technology for Self-Powered Systems and as Active Mechanical and Chemical Sensors.* ACS Nano, 2013. 7(11): p. 9533-9557.
4. Fan, F.-R., Z.-Q. Tian, and Z. Lin Wang, *Flexible triboelectric generator.* Nano Energy, 2012. 1(2): p. 328-334.
5. Davies, D.K., *Charge generation on dielectric surfaces.* Journal of Physics D: Applied Physics, 1969. 2(11): p. 1533.
6. Wang, Z.L., J. Chen, and L. Lin, *Progress in triboelectric nanogenerators as a new energy technology and self-powered sensors.* Energy & Environmental Science, 2015. 8(8): p. 2250-2282.
7. Xue, X., et al., *Hybridizing Energy Conversion and Storage in a Mechanical-to-Electrochemical Process for Self-Charging Power Cell.* Nano Letters, 2012. 12(9): p. 5048-5054.
8. Xue, X., et al., *CuO/PVDF nanocomposite anode for a piezo-driven self-charging lithium battery.* Energy & Environmental Science, 2013. 6(9): p. 2615-2620.
9. Xue, X., et al., *Flexible Self-Charging Power Cell for One-Step Energy Conversion and Storage.* Advanced Energy Materials, 2014. 4(5): p. n/a-n/a.

10. Zhang, Y., et al., *PVDF–PZT nanocomposite film based self-charging power cell* Nanotechnology, 2014. 25(10): p. 105401.

11. Xing, L., et al., *PVDF mesoporous nanostructures as the piezo-separator for a self-charging power cell.* Nano Energy, 2014. 10: p. 44-52.

12. Ramadoss, A., et al., *Piezoelectric-Driven Self-Charging Supercapacitor Power Cell.* ACS Nano, 2015. 9(4): p. 4337-4345.

13. Coyle, S., et al., *Smart Nanotextiles: A Review of Materials and Applications.* MRS Bulletin, 2007. 32(05): p. 434-442.

14. Rahman, M.A., et al., *Fabrication and characterization of highly efficient flexible energy harvesters using PVDF–graphene nanocomposites* Smart Materials and Structures, 2013. 22(8): p. 085017.

15. Wang, Z.L., *From nanogenerators to piezotronics—A decade-long study of ZnO nanostructures.* MRS Bulletin, 2012. 37(09): p. 814-827.

16. Wei, W., et al., *Manganese oxide-based materials as electrochemical supercapacitor electrodes.* Chemical Society Reviews, 2011. 40(3): p. 1697-1721.

17. Toupin, M., T. Brousse, and D. Bélanger, *Influence of Microstucture on the Charge Storage Properties of Chemically Synthesized Manganese Dioxide.* Chemistry of Materials, 2002. 14(9): p. 3946-3952.

18. Toupin, M., T. Brousse, and D. Bélanger, *Charge Storage Mechanism of MnO2 Electrode Used in Aqueous Electrochemical Capacitor.* Chemistry of Materials, 2004. 16(16): p. 3184-3190.

19. Xia, J., et al., *Measurement of the quantum capacitance of graphene.* Nat Nano, 2009. 4(8): p. 505-509.

20. Ramadoss, A., B. Saravanakumar, and S.J. Kim, *Thermally reduced graphene oxide-coated fabrics for flexible supercapacitors and self-powered systems.* Nano Energy, 2015. 15: p. 587-597.

21. Bolotin, K.I., et al., *Ultrahigh electron mobility in suspended graphene.* Solid State Communications, 2008. 146(9–10): p. 351-355.

22. Stoller, M.D., et al., *Graphene-Based Ultracapacitors.* Nano Letters, 2008. 8(10): p. 3498-3502.

23. Pei, S. and H.-M. Cheng, *The reduction of graphene oxide.* Carbon, 2012. 50(9): p. 3210-3228.

24. Yu, G., et al., *Solution-Processed Graphene/MnO2 Nanostructured Textiles for High-Performance Electrochemical Capacitors.* Nano Letters, 2011. 11(7): p. 2905-2911.

25. Liu, W.-w., et al., *Flexible and conductive nanocomposite electrode based on graphene sheets and cotton cloth for supercapacitor.* Journal of Materials Chemistry, 2012. 22(33): p. 17245-17253.

26. Wang, Y.-S., et al., *Integration of tailored reduced graphene oxide nanosheets and electrospun polyamide-66 nanofabrics for a flexible supercapacitor with high-volume- and high-area-specific capacitance.* Carbon, 2014. 73: p. 87-98.

27. Lin Wang, Z. *Self-powered nanosystem: From nanogenerators to piezotronics*. in *Solid-State and Integrated Circuit Technology (ICSICT), 2010 10th IEEE International Conference on*. 2010.

28. Wang, Z.L. and J. Song, *Piezoelectric Nanogenerators Based on Zinc Oxide Nanowire Arrays.* Science, 2006. 312(5771): p. 242-246.

29. Ikjoo, B., W.C. Anthony, and K. Beomjoon, *Transfer of thin Au films to polydimethylsiloxane (PDMS) with reliable bonding using (3-*

mercaptopropyl)trimethoxysilane (MPTMS) as a molecular adhesive. Journal of Micromechanics and Microengineering, 2013. 23(8): p. 085016.

30. Kaniyoor, A. and S. Ramaprabhu, *A Raman spectroscopic investigation of graphite oxide derived graphene.* AIP Advances, 2012. 2(3): p. 032183.
31. Tuinstra, F. and J.L. Koenig, *Raman Spectrum of Graphite.* The Journal of Chemical Physics, 1970. 53(3): p. 1126-1130.
32. Stankovich, S., et al., *Synthesis of graphene-based nanosheets via chemical reduction of exfoliated graphite oxide.* Carbon, 2007. 45(7): p. 1558-1565.
33. King, A.A.K., et al., *A New Raman Metric for the Characterisation of Graphene oxide and its Derivatives.* Scientific Reports, 2016. 6: p. 19491.
34. Ambrosi, A., et al., *Electrochemistry at Chemically Modified Graphenes.* Chemistry – A European Journal, 2011. 17(38): p. 10763-10770.
35. Kundu, S., et al., *Thermal Stability and Reducibility of Oxygen-Containing Functional Groups on Multiwalled Carbon Nanotube Surfaces: A Quantitative High-Resolution XPS and TPD/TPR Study.* The Journal of Physical Chemistry C, 2008. 112(43): p. 16869-16878.
36. Gupta, B., et al., *Role of oxygen functional groups in reduced graphene oxide for lubrication.* Scientific Reports, 2017. 7: p. 45030.
37. Wang, Z., et al., *Graphene Oxide Filled Nanocomposite with Novel Electrical and Dielectric Properties.* Advanced Materials, 2012. 24(23): p. 3134-3137.
38. Islam, R., et al., *Evidence of interfacial charge trapping mechanism in polyaniline/reduced graphene oxide nanocomposites.* Applied Physics Letters, 2015. 107(5): p. 053102.

39. Yaqoob, U., A.S.M.I. Uddin, and G.-S. Chung, *The effect of reduced graphene oxide on the dielectric and ferroelectric properties of PVDF-BaTiO3 nanocomposites.* RSC Advances, 2016. 6(36): p. 30747-30754.

40. Yuan, J., et al., *Graphene liquid crystal retarded percolation for new high-k materials.* Nat Commun, 2015. 6.

41. Stankovich, S., et al., *Graphene-based composite materials.* Nature, 2006. 442(7100): p. 282-286.

42. Glover, A.J., D.H. Adamson, and H.C. Schniepp, *Charge-Driven Selective Adsorption of Sodium Dodecyl Sulfate on Graphene Oxide Visualized by Atomic Force Microscopy.* The Journal of Physical Chemistry C, 2012. 116(37): p. 20080-20085.

43. Hsieh, A.G., et al., *Dispersion Stability of Functionalized Graphene in Aqueous Sodium Dodecyl Sulfate Solutions.* Langmuir, 2013. 29(48): p. 14831-14838.

44. Hsieh, A.G., et al., *Adsorption of Sodium Dodecyl Sulfate on Functionalized Graphene Measured by Conductometric Titration.* The Journal of Physical Chemistry B, 2013. 117(26): p. 7950-7958.

45. Tummala, N.R., B.P. Grady, and A. Striolo, *Lateral confinement effects on the structural properties of surfactant aggregates: SDS on graphene.* Physical Chemistry Chemical Physics, 2010. 12(40): p. 13137-13143.

46. Onogi, Y., N. Sugiura, and C. Matsuda, *Temperature Effect on Dissipation of Triboelectric Charge into Air from Textile Surfaces.* Textile Research Journal, 1997. 67(1): p. 45-49.

47. Niu, S., et al., *Theoretical study of contact-mode triboelectric nanogenerators as an effective power source.* Energy & Environmental Science, 2013. 6(12): p. 3576-3583.

Appendix

Viyada Harnchana, Van Huynh Ngoc, Wen He, Aamir Rashhed, Hyunje Park, Vittaya Amornkitbamrung, and Dae Joon Kang, Enhanced Power Output of a Triboelectric Nanogenerator using Polydimethylsiloxane Modified with Graphene Oxide and Sodium Dodecyl sulfate, ACS applied materials and interfaces, article ASAP (2018)

ACS APPLIED MATERIALS & INTERFACES

Research Article

Cite This: ACS Appl. Mater. Interfaces XXXX, XXX, XXX−XXX

www.acsami.org

Enhanced Power Output of a Triboelectric Nanogenerator using Poly(dimethylsiloxane) Modified with Graphene Oxide and Sodium Dodecyl Sulfate

Viyada Harnchana,[†,‡,§,∥] Huynh Van Ngoc,[†] Wen He,[†] Aamir Rasheed,[†] Hyunje Park,[†] Vittaya Amornkitbamrung,[‡,§,∥] and Dae Joon Kang*[,†]

[†]Department of Physics and Institute of Basic Science, Sungkyunkwan University, 2066, Seobu-ro, Suwon-si, Gyeonggi-do 16419, Republic of Korea

[‡]Department of Physics and [§]Integrated Nanotechnology Research Center, Khon Kaen University, Khon Kaen 40002, Thailand

[∥]Nanotec-KKU Center of Excellence on Advanced Nanomaterials for Energy Production and Storage, Khon Kaen 40002, Thailand

Supporting Information

ABSTRACT: In this work, a new approach to modifying poly(dimethylsiloxane) (PDMS) as a negative triboelectric material using graphene oxide (GO) and a sodium dodecyl sulfate (SDS) surfactant was reported. A porous PDMS@GO@SDS composite triboelectric nanogenerator (TENG) could deliver an output voltage and current of up to 438 V and 11 $\mu A/cm^2$, respectively. These values were 3-fold higher than those of the flat PDMS. The superior performance is attributed to the intensified negative charges on PDMS from the oxygen functional groups of GO and anionic head groups of the SDS molecules. The outstanding performance and straightforward, low-cost fabrication process of the PDMS@GO@SDS TENG would be beneficial for the further development of powerful NGs integrated into wearable electronics and self-charging power cells.

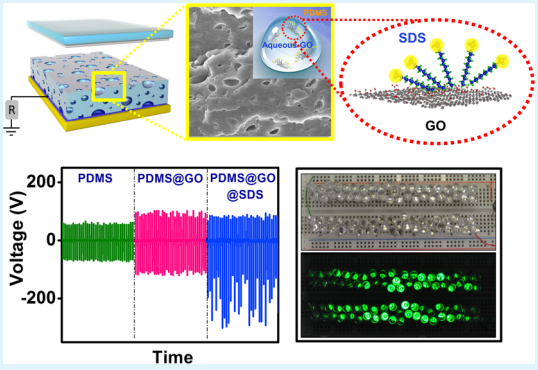

KEYWORDS: *triboelectric, nanogenerator, poly(dimethylsiloxane), graphene oxide and sodium dodecyl sulfate*

1. INTRODUCTION

Harvesting the ubiquitous mechanical energy in ambient environment is one of the most demanding challenges in developing green, sustainable energy sources. Triboelectric nanogenerators (TENGs) are newly developed energy conversion devices with high potential as a power-generation technology because of their high output power and cost-effective fabrication.[1−3] The electric power generation of TENGs is based on triboelectrification and electric induction, which depend on the contact−separation movements of the two triboelectric materials with different triboelectric polarities.[4] Triboelectric materials are coupled according to the large difference in their electronegativities, as presented in the triboelectric series.[5] To realize their practical applications, high-performance flexible and wearable TENGs need to be developed.

Poly(dimethylsiloxane) (PDMS) has been widely used as a negative triboelectric material.[6−11] Although it is the second most negative triboelectric material after poly(tetrafluoroethylene) (PTFE) in the triboelectric series, its demand is higher than PTFE because of its flexibility and transparency. Moreover, PDMS can be mixed with numerous nanostructured materials to form various composite films. In addition, its coating ability on other surfaces is regarded as a significant advantage over PTFE.

In addition to the choice of material, the surface morphology has been established as a crucial factor that enhances electrification because of the increased physical contact area. Many studies have demonstrated that modifying the surface morphology or inner structure of PDMS films can significantly improve the output performance of TENGs. These strategies include surface patterning, including micropatterning,[11] adding chemical functional groups using block copolymers,[12,13] treating PDMS with fluorocarbons,[14] plasma etching,[14] forming a porous sponge structure,[15−17] and adding nanostructured materials.[8,18]

Many high-power-output TENGs have been fabricated through the aforementioned approaches. However, their fabrication processes and device designs were relatively complicated, with some requiring sophisticated synthesis systems. To overcome this limitation, a facile, effective modification method for PDMS films is required to mass-

Received: February 9, 2018
Accepted: July 6, 2018
Published: July 6, 2018

DOI: 10.1021/acsami.8b02495
ACS Appl. Mater. Interfaces XXXX, XXX, XXX−XXX

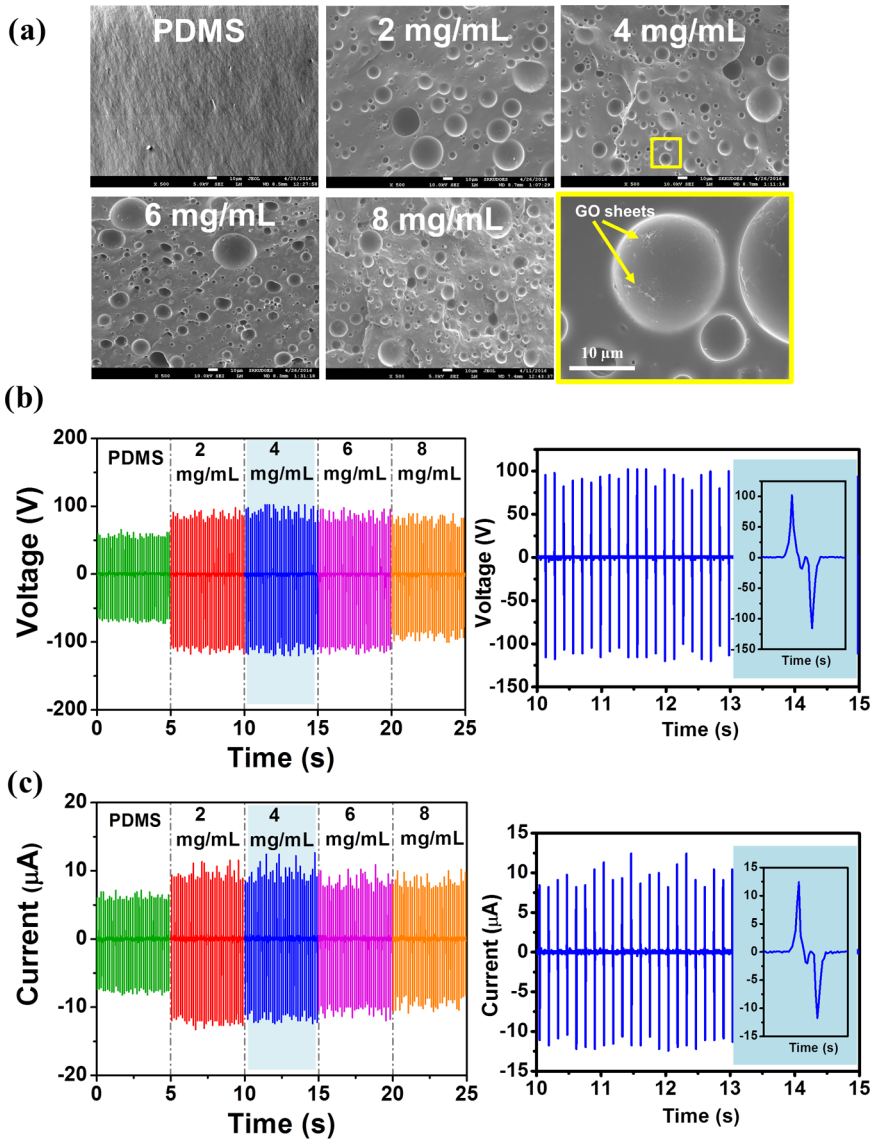

Figure 1. (a) SEM images and the (b) voltage and (c) current output of PDMS and PDMS@GO films with various GO concentrations.

produce high-performance TENGs with reduced production costs.

Graphene oxide (GO) is rich in negative charges because it has oxygen functional groups decorated on both the carbon network basal planes and edges.[19] Thus, it can serve as a negative triboelectric material and offer diverse modifications through its functional groups. The first flexible GO-based NG utilized the charge-storing property of GO to harvest acoustic energy and transform it into electricity, with an energy-conversion efficiency of up to 12.1%.[20] Furthermore, an electrostatic NG based on GO films was fabricated; however, its output performance was relatively low.[21] GO-doped electrospun poly(vinylidene fluoride) nanofibers developed for a book-shaped TENG increased the charge-storage capability and output performance of the device.[22] This charge-trapping mechanism was also reported in a polyaniline/reduced GO (rGO) layerlike core−shell structure, in which electric charges were trapped because of the dissimilar electrical conductivities of polyaniline and rGO.[23]

The study of the electric and dielectric properties of GO-filled PDMS composites showed that the composite exhibited unusual nonlinear electrical conductivity and a high dielectric constant.[24] The use of a PDMS/GO composite as a triboelectric material has been recently reported.[25] The embedded GO nanoparticles in PDMS films acting as charge-trapping sites could increase the relative dielectric property of the films, which were found to exhibit higher TENG output performance than that of a pure PDMS film. In the present study, we employed GO solution to modify the PDMS triboelectric material and enhance its triboelectric properties. In addition to taking advantage of the unique electrical properties of GO, we explored the insolubility of an aqueous GO in the PDMS solution to produce a desirable porous structure, resulting in increased surface contact area, thus enhancing the triboelectric properties.

We also incorporated an anionic surfactant, sodium dodecyl sulfate (SDS), into the GO/PDMS system to pile up the negative charges in the PDMS composite, denoted PDMS@GO@SDS, and enhance the power output of the TENGs. Using this novel approach, we developed a procedure to produce a high-performance TENG using the PDMS@GO@SDS composite, thereby achieving a high output performance

DOI: 10.1021/acsami.8b02495
ACS Appl. Mater. Interfaces XXXX, XXX, XXX−XXX

because of the highly accumulated negative charges and charge transport properties of the composite film. The effects of the concentrations of GO and SDS, film thickness, operation force, and frequency on the output performance of the TENGs were thoroughly investigated. This unprecedented, facile modification approach for PDMS triboelectric materials could be promising for the large-scale production of high-performance TENGs.

2. EXPERIMENTAL SECTION

2.1. Fabrication of PDMS@GO and PDMS@GO@SDS. A PDMS solution (Sylgard 184, Dow Corning) containing both the elastomer and curing agent in a mass ratio of 10:1 was prepared for the flat, pristine PDMS film. GO was prepared using a typical two-step modified Hummer's method.[26,27] For the PDMS@GO composite film, a GO solution with various concentrations (2, 4, 6, and 8 mg/mL) was mixed with a PDMS elastomer solution in a volume ratio of 1:5 through magnetic stirring for 30 min. For simplicity, these samples are hereafter referred to as PDMS@GO-2, PDMS@GO-4, PDMS@GO-6, and PDMS@GO-8, respectively. For the porous PDMS@GO@SDS films, the SDS surfactant was dissolved in the 4 mg/mL GO suspension at concentrations of 0.1, 0.2, 0.3, and 0.4 M before mixing with the elastomer solution, and the corresponding samples are hereafter referred to as PDMS@GO@SDS-0.1, PDMS@GO@SDS-0.2, PDMS@GO@SDS-0.3, and PDMS@GO@SDS-0.4, respectively. Next, the curing agent was added to each suspension, and stirring was resumed for 15 min to obtain a uniformly dispersed solution. The negative electrodes of the TENGs were spin-coated onto a 2 × 2.5 cm^2 Au-coated glass substrate whose surface was underwent a pretreatment step to promote adhesion by immersing in 5 mM (3-mercaptopropyl)trimethoxysilane solution for 30 min.[28] The PDMS composite films were then cured at 80 °C for 2 h, and water was removed at 150 °C for 2 h using a hot plate.

2.2. Characterization. The morphology of the films was examined using a field emission scanning electron microscope (FE-SEM, JSM-7001F, JEOL, Japan) under an operation voltage of 10 kV equipped with an energy-dispersive X-ray (EDX) spectrometer (INCA PentaFETx3, Oxford Instruments, England). The GO content in the fabricated composite films was characterized using a Raman spectrometer system (XperRam Compact, Nanobase with a 532 nm laser excitation) and X-ray photoelectron spectroscopy (XPS, an ESCA Lab2201-XL spectrometer using an Al Kα X-ray as the excitation source). The XPS spectra were calibrated using the C 1s binding energy at 284.6 eV as the reference.

The electrical characteristics of the TENGs were measured using a digital oscilloscope (LeCroy WaveRunner 6100A) and a low-noise current preamplifier (Stanford Research Systems SR570) in the compressive operation mode. The contact−separation movement was created using a pressing test system that can generate the movement with the applied force from 1 to 10 N at 1−10 Hz frequency.

3. RESULTS AND DISCUSSION

First, the effects of GO concentration on the morphology of the PDMS@GO composite films and their voltage and current outputs were investigated under a repeated compressive force of 1 N at 7 Hz. Figure 1a shows the SEM images of the PDMS@GO with 2−8 mg/mL GO. In contrast with flat PDMS, the PDMS@GO films feature porous structures due to the formation of bubbles by the indissoluble GO in the PDMS. Although the porous structures show no significant differences among the various GO concentrations, the pore density increases with the GO concentration. The high-magnification SEM image reveals that the GO sheets were trapped inside the porous structure and well dispersed across their sidewalls; the SEM images of PDMS@GO films with various GO concentrations are shown in the Supporting Information Figure S1. The output performance of the various PDMS@GO films exhibits a notably similar trend, as shown in Figure 1b. As the GO concentration increases, the output voltage and current reach their maximum values of 215 V and 6 $\mu A/cm^2$, respectively, with the 4 mg/mL GO sample. The outputs then decrease with the increased GO concentrations of 6 and 8 mg/mL, which could be attributed to the aggregation of GO, which will be further discussed in the following part.

To elucidate the lower performance at high GO concentrations in the PDMS@GO composite films, Raman spectroscopy analysis was performed, as presented in Figure 2a. The

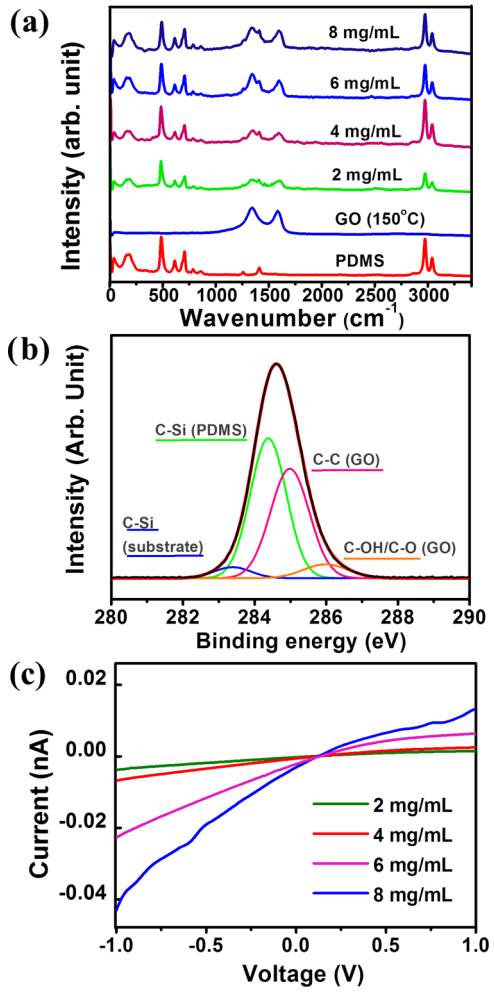

Figure 2. (a) Raman spectra of the PDMS and PDMS@GO films with various GO concentrations, (b) C 1s X-ray photoelectron spectra of the 4 mg/mL PDMS@GO composite film, and (c) $I-V$ measurements of the composite films.

characteristic Raman spectrum of PDMS is consistent with that in the relevant literature. The two peaks at 1345 and 1595 cm^{-1} are assigned to the disorder-induced D bands and in-plane C−C stretching G bands of GO, respectively. The Raman spectra of the composite films contain the superimposed spectra of both PDMS and GO with no additional peaks, which are further supported by the Fourier transform infrared (FTIR) data in Figure S2 in the Supporting Information, suggesting that no chemical interaction occurred between the two components. The Raman spectra of two pristine GO films heated at 80 and 150 °C were acquired to probe the transformation of GO during the fabrication process.

DOI: 10.1021/acsami.8b02495
ACS Appl. Mater. Interfaces XXXX, XXX, XXX−XXX

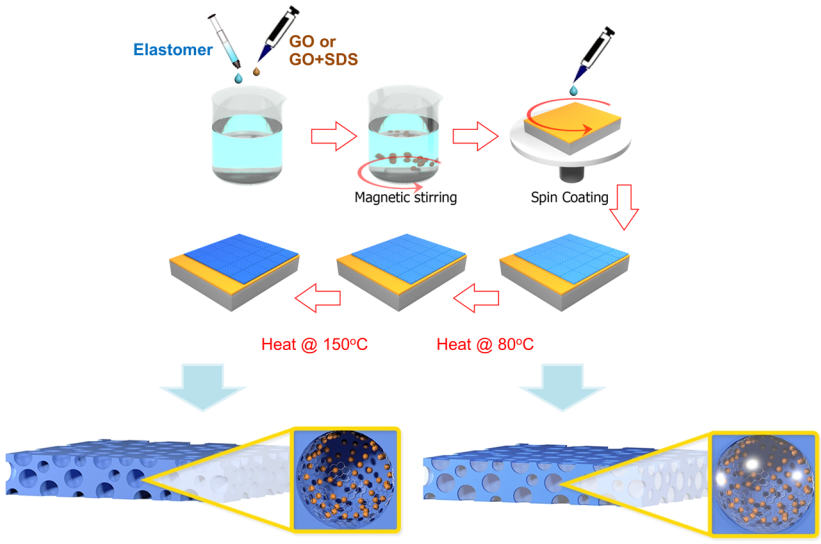

Figure 3. Schematic illustrating the fabrication of PDMS@GO films as negative triboelectric materials.

The I_D/I_G ratios that can be used as the measure of defect/disorder density in GO were found to slightly increase from ~1.0 to ~1.1 in the 80 and 150 °C heated GO (representing the composite films at all GO concentrations), respectively (Supporting Information Figure S3).[29−31] These numbers are still lower than those determined in some previous studies[32,33] suggesting that GO was partially reduced, forming rGO, but the degree of reduction was relatively low. The increase in the D peak intensity after the 150 °C heating indicates that more oxygen functional groups were introduced into carbon chains, which could be surface hydroxyl and/or epoxy groups from vaporized water.[34]

To support the Raman data, a C 1s XPS spectrum was acquired from the best-performing PDMS@GO-4 composite film (the 4 mg/mL GO film), as presented in Figure 2b. The deconvoluted C 1s XPS spectrum reveals four C components in the composite. The C−C and C−OH/C−O components at ~285 and ~286 eV are from covalent carbon bonds and hydroxyl/epoxy groups, respectively.[34,35] Two other C−Si components at ~283.5 and 284.5 eV are obtained from the bonding between the C and Si atoms in the substrate and in the PDMS molecules, respectively. The intensity ratio of the C−C and C−O components (I_{C-C}/I_{C-O}) in the XPS spectrum verifies the reduction of GO, which forms rGO in the composite.

The fabrication steps and a proposed model of the porous PDMS@GO composite are shown in Figure 3. In the PDMS@GO composite film, because the aqueous GO suspension cannot be dissolved in the PDMS prepolymer, small droplets of GO solution can be dispersed inside the PDMS matrix with the help of an SDS surfactant that promotes emulsification of the mixture solution under magnetic stirring. Next, annealing is performed (i) at 80 °C to cure the PDMS film and (ii) at 150 °C to evaporate the water trapped inside the droplets. Annealing at 150 °C in the ambient atmosphere has synergistic effects: removing the confined water bubbles produces the porous film and introduces more oxygen functional groups into carbon chains of GO from the vaporized water. The increased specific surface area of the porous structure decorated with rich oxygen functional groups of GO can provide more negative surface charge to the composite film. Furthermore, the heat treatment may also promote the restoring of the carbon hexagonal network, which results in the partial reduction of GO. Although rGO contains lesser oxygen functional groups than GO, its restored carbon network can improve the conductivity, as evidenced by the decrease of electrical resistance in Figure 2c. The rGO clusters in the insulating the PDMS matrix act as charge-trapping sites that can induce a capacitance effect, which has also been observed in previous studies.[23,24,36,37] These synergistic effects account for the improved output performance of the PDMS@GO TENG.

However, the decreased output performance at higher GO concentration can be ascribed to the aggregation of rGO resulting in the electrical percolation of the rGO network in the PDMS matrix,[38,39] as evidenced by the increasing conductivity shown in the current−voltage ($I-V$) measurements in Figure 2c. The resistances of all of the composite films were relatively high (10^9 Ω) and decreased with the increasing GO concentration. The higher GO precursor concentrations resulted in the connection of the conductive rGO network, as shown in the SEM images of the dense porous structure in the fabricated PDMS@GO-6 and PDMS@GO-8 films in Figure 1a. The electrical percolation directly affects the output performance of the composite TENGs because of the dissipation of electrified charges, thus resulting in a decrease in the potential and current output.

The PDMS@GO films exhibit relatively wide size distributions of bubbles or pores, which range in diameter from a few micrometers to a few tens of micrometers. We added the SDS surfactant to emulsify GO in the PDMS matrix for ensuring the formation of a desirable porous structure by homogeneously dispersing the GO clusters into the PDMS matrix, which resulted in enhancement of the specific contact area. Moreover, the anionic head groups of the SDS molecules were expected to further intensify the negative charges in the composite films. Figure 4a presents the effect of the SDS concentration on the output performance of the PDMS@GO@SDS TENGs. The highest output voltage and current of up to 330 V and 8 $\mu A/cm^2$, respectively, were achieved for PDMS@GO@SDS with 0.2 M SDS. This can power 90 green light emitting diodes (LEDs), as shown in Figure 4b and Video S5 in the Supporting Information. The achieved output performance was approximately 1.5 times greater than that of the PDMS@GO-4 TENG. At high SDS concentrations, the

DOI: 10.1021/acsami.8b02495
ACS Appl. Mater. Interfaces XXXX, XXX, XXX−XXX

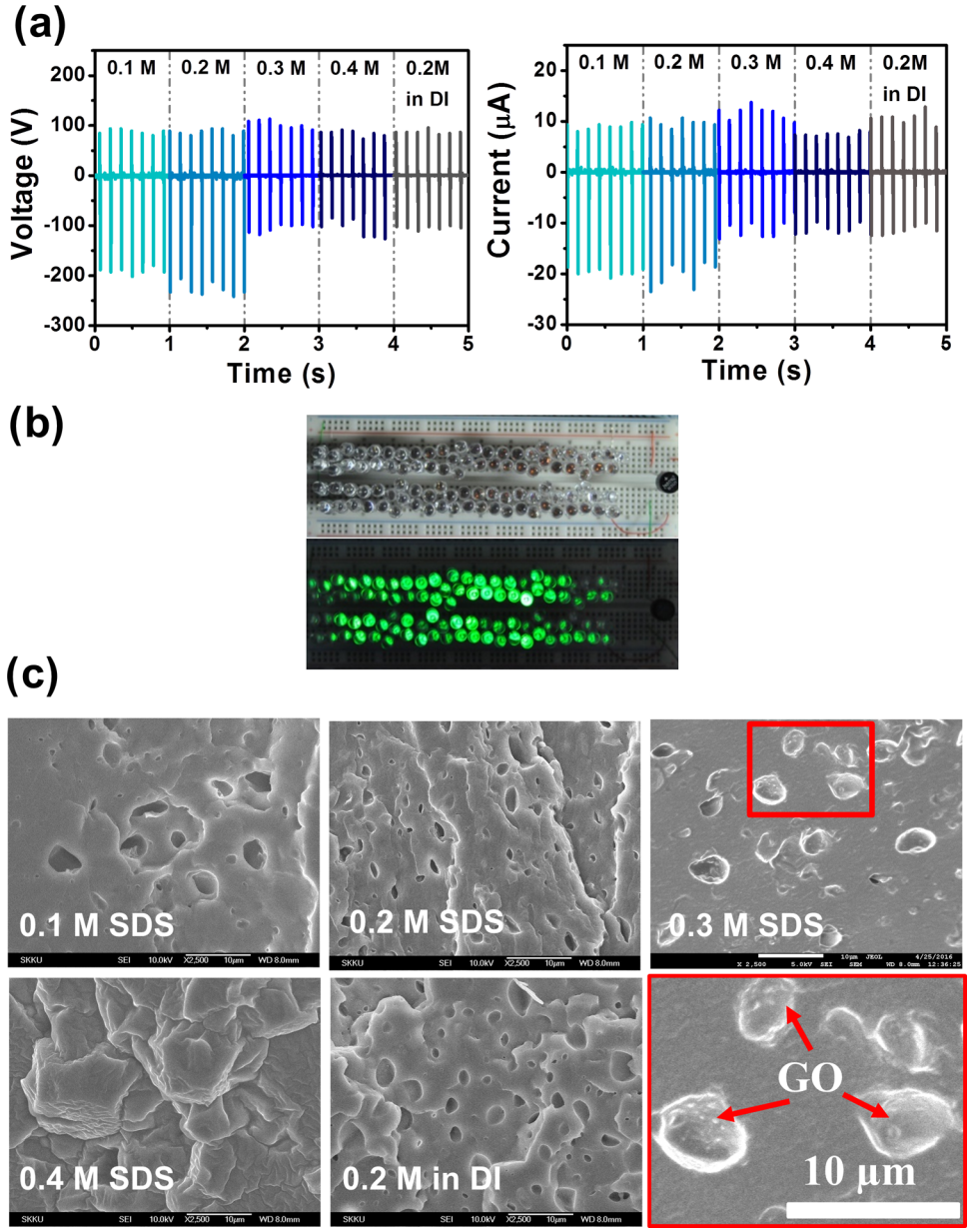

Figure 4. (a) Output voltage and current of the PDMS@GO@SDS composite TENG with various SDS concentrations; (b) 90 LEDs can be illuminated using 0.2 M SDS PDMS@GO@SDS TENG; and (c) SEM images of the PDMS@GO@SDS composite films with various SDS concentrations, with the magnified red rectangular region indicating the presence of GO inside the pores.

output performance deteriorated to almost the same output as that of the PDMS@GO without SDS. The SEM images shown in Figure 4c reveal the remarkable changes in morphology among the PDMS@GO@SDS samples with various SDS concentrations; the enlarged image of the red rectangular region indicates the presence of GO inside the pores.

When the SDS surfactant is initially added to the GO solution prior to being mixed with the PDMS prepolymer, the hydrophilic negatively charged head groups of the SDS molecules are electrostatically repelled from the negatively charged oxygen-containing functional groups on the GO surface. Thus, SDS molecules are not adsorbed onto the GO but form micelles in the solution.[40] In contrast, SDS alkyl chains have been demonstrated to adsorb on rGO surfaces, and their absorption behavior was found to depend on the SDS concentration and the degree of GO reduction.[41,42] In this study, the SDS concentration is relatively higher than the typical critical surface aggregation concentration reported in previous studies.[41,42] The SDS molecules are expected to form hemicylindrical and/or hemispherical surface micelles[43] and micelles in bulk solution. If the SDS concentration is extremely high (0.4 M), the morphology of the composite becomes granular and discontinuous, thus deteriorating the output performance of the TENGs.

Figure 5 shows the SEM-EDX mapping of S Kα_1, C K$\alpha_{1,2}$, and Si Kα_1 in the PDMS@GO@SDS. Sulfur was detected across the sample with some porosity, suggesting the uniform dispersion of the SDS molecules in the composite and the micelle formation in the precursor solution. However, the yellow circles and arrows in Figure 5a,b indicate areas of high sulfur density, suggesting the presence of rGO with adsorbed SDS molecules located close to the holes. This could indicate

DOI: 10.1021/acsami.8b02495
ACS Appl. Mater. Interfaces XXXX, XXX, XXX−XXX

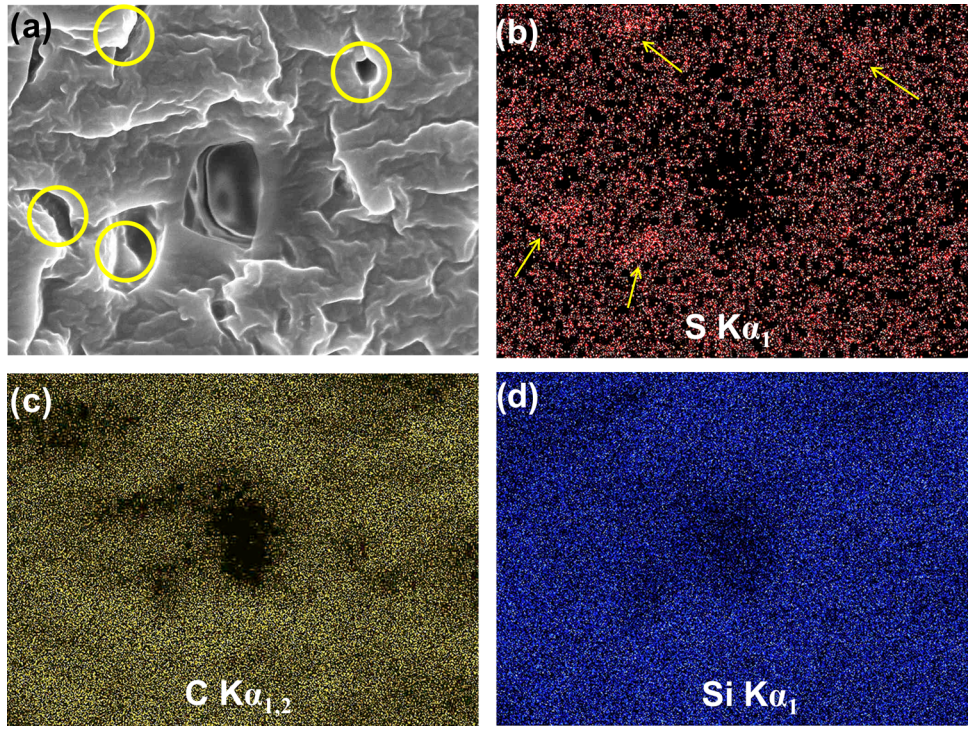

Figure 5. (a) SEM image and SEM-EDX mappings of (b) S Kα_1, (c) C K$\alpha_{1,2}$, and (d) Si Kα_1 in the PDMS@GO@SDS film with 0.2 M SDS concentration.

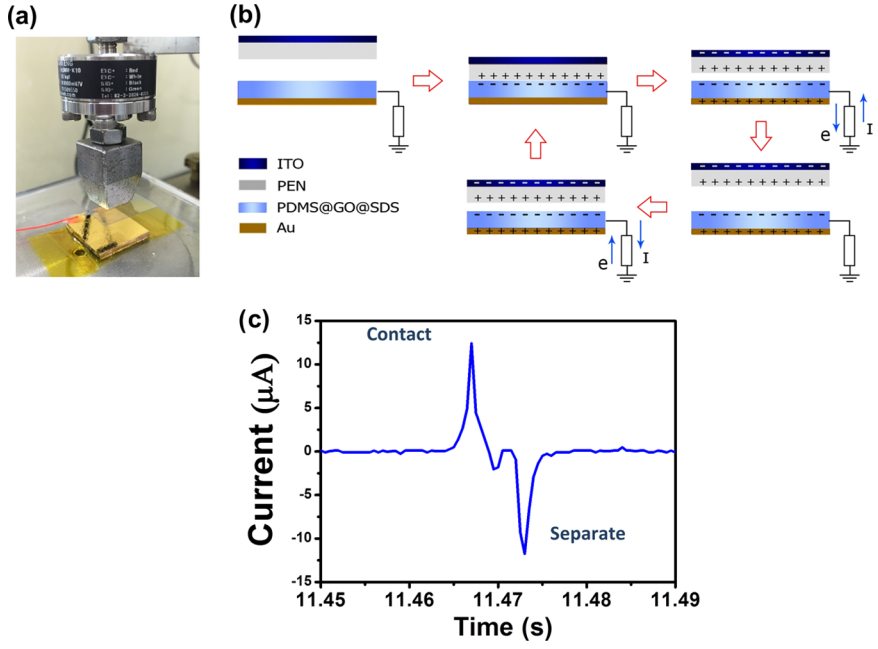

Figure 6. (a) Output measurement, (b) schematic presentation of the working principle of the fabricated TENG in the single-electrode mode, and (c) measured current output signal.

the presence of rGO on the sidewalls of the pores. The dispersion of GO sheets in the PDMS film is also evidenced by TEM images in Figure S4 in the Supporting Information where GO sheets were observed around the pore regions as well as inside the PDMS matrix.

The working principle of the fabricated PDMS@GO@SDS TENG under a single-electrode mode is presented with the output measurement setup in Figure 6, using a polyethylene naphthalate (PEN) film with indium tin oxide (ITO) deposited on the top as a moving electrode with the PEN side facing the PDMS@GO@SDS film, which was spin-coated on a Au-coated glass substrate. In the initial state, the two film surfaces are not in contact, no charge transfer occurs, and hence no electric potential exists. When the two materials are brought into contact, electrons transfer between the PEN and PDMS films upon electrification, producing positive and negative charges at the surfaces of the PEN and PDMS@

DOI: 10.1021/acsami.8b02495
ACS Appl. Mater. Interfaces XXXX, XXX, XXX−XXX

Table 1. Maximum Voltage and Current Outputs Extract from Output Signals in Figures 1, 4, 7, and 8 and Their Corresponding Transfer Charge Densities

material	synthesis condition	frequency (Hz)	V_{oc} (V)	current (peak to peak) (μA)	transfer charge $\Delta\sigma$ (μC/m^2)	
					contact	separate
PDMS	flat	5	125	14	28	32
PDMS@GO	GO 2 mg/mL	5	204	24	39	45
	GO 4 mg/mL	5	218	25	42	45
	GO 6 mg/mL	5	204	20	40	42
	GO 8 mg/mL	5	173	19	32	36
PDMS@GO@SDS (GO 4 mg/mL)	SDS 0.1 M	5	278	30	41	56
	SDS 0.2 M	5	331	33	41	60
	SDS 0.3 M	5	226	23	41	58
	SDS 0.4 M	5	213	19	30	42
PDMS@GO@SDS (GO 4 mg/mL) (SDS 0.2 M)		1	200	16	29	39
		2	188	21	41	56
		3	230	24	43	58
		4	246	25	43	56
		5	317	35	43	59
		6	342	37	39	56
		7	377	44	38	58
		8	412	45	36	53
		9	215	26	31	39
		10	213	26	28	37

GO@SDS films, respectively, as a result of the chemical potential difference.

When the two surfaces are separated, the electric potential created by the triboelectric charges on the surfaces drives free electrons in the bottom Au electrode to flow to the ground to neutralize the negative charges on the composite film, leaving a positively charged Au electrode and generating a negative voltage signal. Simultaneously, the positive charges on the PEN surface can induce free electrons in the ITO top layer to accumulate at the interface without tunneling through the PEN film. In the single-electrode operation mode, the ITO is not directly connected to the bottom Au electrode; this configuration provides electrostatic capacitive effect that can confine or keep positive surface charges to remain on the PEN surface during the separation stage; otherwise, some of the electrified charges can dissipate into the atmosphere due to water molecules in the air.[44] When the two surfaces are brought back into contact again, the potential experienced by the free electrons in the bottom electrode decreases, and they thus flow back from the ground to neutralize the earlier positively charged Au electrode, producing a positive voltage signal.

In this study, the output performance was significantly augmented by increasing the charge density. Considering a simple contact mode operation, the output voltage (V) and the voltage at the open circuit (V_{oc}), with no transferred charge, are given by eqs 1 and 2.[45]

$$V = \frac{(\sigma_0 - \Delta\sigma)\cdot x(t)}{\varepsilon_0} - \frac{\Delta\sigma\cdot d}{\varepsilon_0\varepsilon_r} \quad (1)$$

$$V_{oc} = \frac{\sigma_0\cdot x(t)}{\varepsilon_0} \quad (2)$$

where σ_0, $\Delta\sigma$, $x(t)$, ε_0, d, and S represent the triboelectric charge density on the film surface, transferred charge density on the electrode, distance between the surfaces of two triboelectric materials, vacuum permittivity, triboelectric film thickness, and the film surface area, respectively.

The maximum voltage, V_{oc}, that can be achieved at the maximum distance between the two triboelectric material surfaces is governed by the triboelectric charge density, σ_0. In this study, the superior output performance of the fabricated TENG is attributed to the synergetic contributions of the PDMS@GO@SDS composite film. First, the oxygen functional groups in the rGO and the anionic head groups of the SDS surfactant molecules provide abundant negative charges. Second, the improved dispersion of rGO in the PDMS results in the increased contact surface area of the sub-10 μm porous structure.

The transfer charges, $\Delta\sigma$, were obtained from the integration of the output current plots ($\Delta\sigma = I\Delta t$) with the use of 10 MΩ input load resistance, and the measured $\Delta\sigma$ values of all samples are presented in Table 1. The charges transfer from ground to the electrode during contact state and from the electrode to ground during separation state, as illustrated in Figure 6b,c. The transfer charge was the highest at the PDMS with 4 mg/mL GO and 0.1 M SDS, which corresponded to its highest output current density.

To further optimize the performance of the composite TENG, the effects of the film thickness, operation force, and contact−separation frequency on the TENG performance were investigated. In addition, the triboelectric charge density, σ, is dependent on the capacitance, C, of the TENG, relative dielectric constant (ε_r), surface area (S), and thickness of the dielectric film (d), as described by eqs 3 and 4.

$$\sigma_0 = \frac{C\Delta V}{S} = \frac{\varepsilon_0\varepsilon_r\Delta V}{d} \quad (3)$$

or

$$C = \frac{\varepsilon_0\varepsilon_r S}{d} \quad (4)$$

DOI: 10.1021/acsami.8b02495
ACS Appl. Mater. Interfaces XXXX, XXX, XXX−XXX

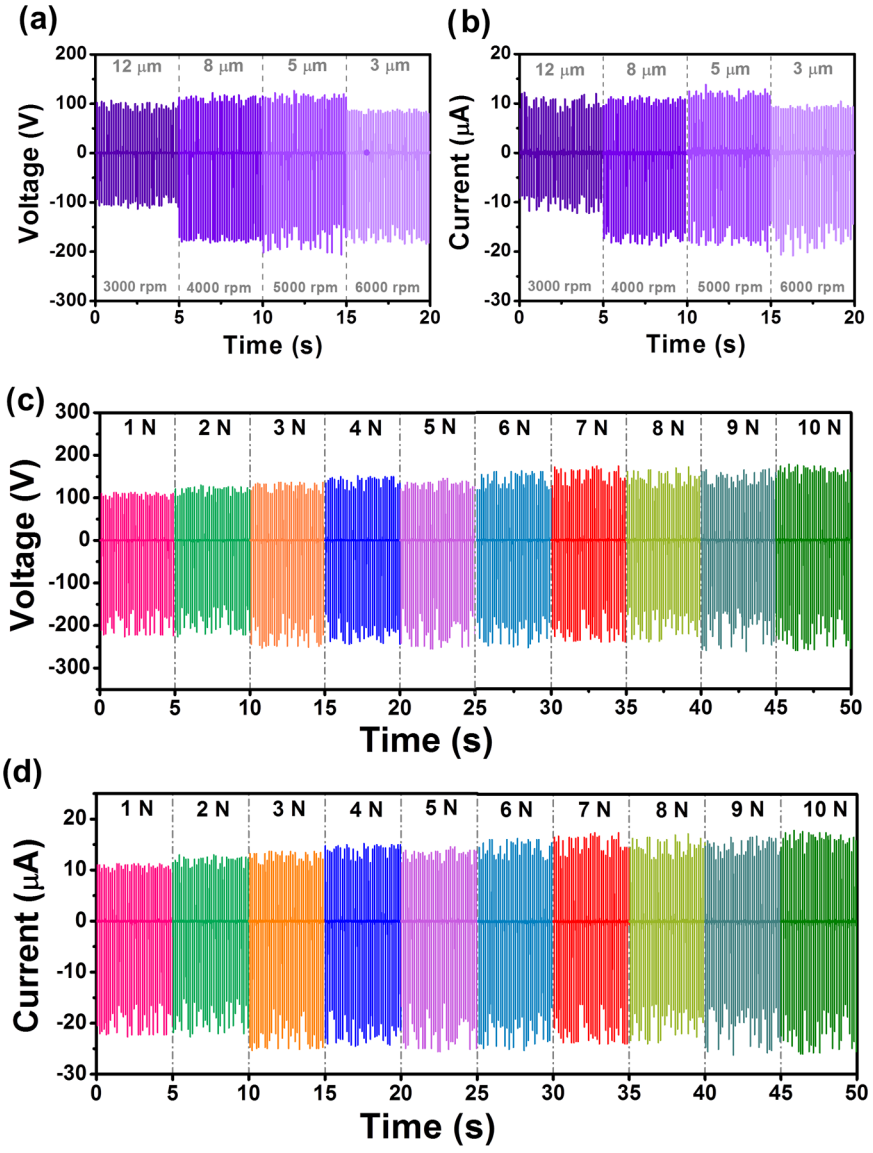

Figure 7. Dependence of the PDMS@GO@SDS TENG output voltage and current on the film thickness (a, b) and the applied force (c, d).

According to these equations, a thin film is expected to exhibit a high performance. However, the optimum film thickness that can produce the highest output performance was determined to be 5 μm, as shown in Figure 7a,b. The thinner film degraded the TENG performance because of the small number of charges. The output performance of the PDMS@GO@SDS TENG gradually increased with the applied force from 1 to 10 N at an operation frequency of 7 Hz with a 5 μm-thick film (Figure 7c,d). The output voltage and current both increase gradually and become almost stable after 6 N. This could be because at 6 N, the applied force provides the maximum frictional contact of the surface and inner structure of the porous composite film.

The frequency dependence was also investigated with a 5 μm-thick film and a constant force of 6 N, as presented in Figure 8; the output performance increases with the operation frequency up to 8 Hz, when the maximum output voltage and current of up to 438 V and 11 μA/cm^2 are achieved, respectively, as shown in Figure 8a,b and Video S6 in the Supporting Information. This dependence could be due to the accumulation of surface charges (σ_0) on the composite material surface that could not be completely neutralized at a high frequency, which can be seen from the reduced transfer charges starting at the frequency of 6 Hz in Table 1. However, at higher operation frequencies of 9 and 10 Hz, the performance dramatically dropped. This could be attributed to the extremely high number of accumulated surface charges, σ_0, generating a strong electric field, which would lead to the air breakdown,[46,47] which can limit the retainable surface charge density. Consequently, the output voltage and current were reduced accordingly.

The effective power density of the TENG can be estimated from the formula $P = V^2/RA$, where V is the output voltage, R is the load resistance, and A is effective size of the TENG. For our output measurement, the input resistance of the oscilloscope is 10 MΩ, and the maximum output power density of the PDMS@GO@SDS is then ~4.8 mW/cm^2.

Table 2 summarizes the output performance under a compressive force of 1 N at 7 Hz. The addition of only GO or SDS demonstrated relatively similar performance; however, when both GO and SDS were mixed into the PDMS to form a PDMS@GO@SDS composite, the output performance greatly

DOI: 10.1021/acsami.8b02495
ACS Appl. Mater. Interfaces XXXX, XXX, XXX−XXX

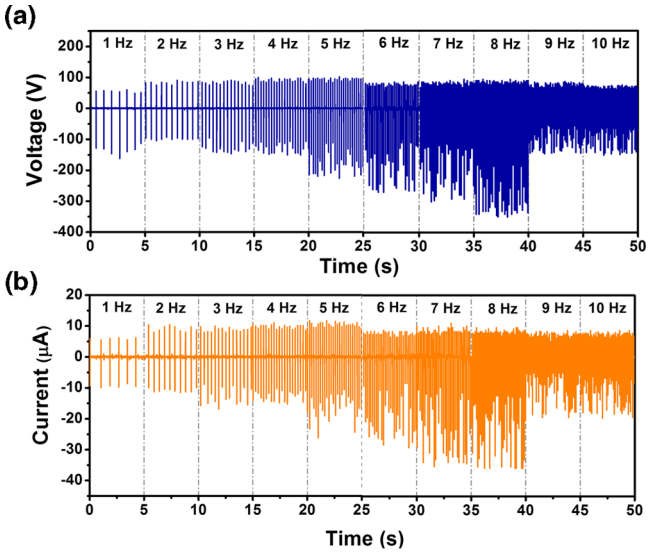

Figure 8. Dependence of the PDMS@GO@SDS TENG output (a) voltage and (b) current on contact−separation frequency.

Table 2. Output Performance Summary at Pressing Operation under 1 N of Force at 7 Hz

samples	voltage (V)	current (μA)
PDMS	131	14
PDMS@GO	215	25
PDMS@GO@SDS	330	32
PDMS@SDS (water)	198	22

improved to almost 3 times that of the flat PDMS film. This order of improvement is consistent with that of other previous studies on enhanced capacitance effect in triboelectric PDMS films such as using aligned graphene sheets embedded in PDMS films[37] and filling high dielectric nanoparticles into sponge PDMS films.[17]

4. CONCLUSIONS

A PDMS@rGO@SDS composite film was successfully developed as a high-performance negative triboelectric material. Under the optimum operating conditions, an output performance 3 times greater than that of a flat PDMS film was achieved, namely, a maximum output voltage and current of 438 V and 11 μA/cm^2, respectively. The negative charge density was intensified by the SDS surfactant and rGO, and the latter also provided enhanced charge trapping. These improvements, in combination with the high contact area of the porous structure, account for the superior output performance of the PDMS@rGO@SDS composite film. This novel approach is conducive to the facile, scalable production of high-performance TENGs.

■ ASSOCIATED CONTENT

Supporting Information

The Supporting Information is available free of charge on the ACS Publications website at DOI: 10.1021/acsami.8b02495.

High-magnification SEM images of the PDMS@GO composite films at various GO concentrations reveal the presence of GO sheets on the pore sidewalls (Figure S1); Fourier transform infrared spectroscopy (FTIR) spectra of the pristine PDMS, PDMS@GO, and PDMS@GO@SDS composited films and GO (Figure S2); Raman spectra of pristine GO films present the change of I_D/I_G ratios during the fabrication process, suggesting that more oxygen functional groups were introduced into the carbon network (Figure S3); TEM images showing the dispersion of GO sheets in porous PDMS matrix in the PDMS@GO@SDS sample (Figure S4) (PDF)

Performance of the PDMS@GO@SDS triboelectric nanogenerator in lighting up LED (Video S5) (AVI)

Output measurement of the PDMS@GO@SDS triboelectric nanogenerator (Video S6) (AVI)

■ AUTHOR INFORMATION

Corresponding Author

*E-mail: djkang@skku.edu. Tel: +82-10-9905-0532. Fax: +82-31-290-5947.

ORCID

Viyada Harnchana: 0000-0002-2686-1701

Dae Joon Kang: 0000-0002-4030-4071

Notes

The authors declare no competing financial interest.

■ ACKNOWLEDGMENTS

This work was supported by the National Research Foundation of Korea grant funded by the Korean government (NRF-2014R1A2A1A11052965). V.H. gratefully acknowledges the support from the Nanotechnology Center (NANOTEC), NSTDA, Ministry of Science and Technology, Thailand, through its program of Center of Excellence Network, the Integrated Nanotechnology Research Center, Khon Kaen University, and Thailand research fund (MRG 5980257).

■ REFERENCES

(1) Hinchet, R.; Seung, W.; Kim, S.-W. Recent Progress on Flexible Triboelectric Nanogenerators for SelfPowered Electronics. *ChemSusChem* **2015**, *8*, 2327−2344.

(2) Ha, M.; Park, J.; Lee, Y.; Ko, H. Triboelectric Generators and Sensors for Self-Powered Wearable Electronics. *ACS Nano* **2015**, *9*, 3421−3427.

(3) Wang, Z. L. Triboelectric Nanogenerators as New Energy Technology for Self-Powered Systems and as Active Mechanical and Chemical Sensors. *ACS Nano* **2013**, *7*, 9533−9557.

(4) Fan, F.-R.; Tian, Z.-Q.; Lin Wang, Z. Flexible triboelectric generator. *Nano Energy* **2012**, *1*, 328−334.

(5) Davies, D. K. Charge generation on dielectric surfaces. *J. Phys. D: Appl. Phys.* **1969**, *2*, 1533.

(6) Zhu, G.; Lin, Z.-H.; Jing, Q.; Bai, P.; Pan, C.; Yang, Y.; Zhou, Y.; Wang, Z. L. Toward Large-Scale Energy Harvesting by a Nanoparticle-Enhanced Triboelectric Nanogenerator. *Nano Lett.* **2013**, *13*, 847−853.

(7) Dudem, B.; Ko, Y. H.; Leem, J. W.; Lee, S. H.; Yu, J. S. Highly Transparent and Flexible Triboelectric Nanogenerators with Subwavelength-Architectured Polydimethylsiloxane by a Nanoporous Anodic Aluminum Oxide Template. *ACS Appl. Mater. Interfaces* **2015**, *7*, 20520−20529.

(8) He, X.; Guo, H.; Yue, X.; Gao, J.; Xi, Y.; Hu, C. Improving energy conversion efficiency for triboelectric nanogenerator with capacitor structure by maximizing surface charge density. *Nanoscale* **2015**, *7*, 1896−1903.

(9) Wang, X.; Yang, B.; Liu, J.; Zhu, Y.; Yang, C.; He, Q. A flexible triboelectric-piezoelectric hybrid nanogenerator based on P(VDF-TrFE) nanofibers and PDMS/MWCNT for wearable devices. *Sci. Rep.* **2016**, *6*, No. 36409.

DOI: 10.1021/acsami.8b02495
ACS Appl. Mater. Interfaces XXXX, XXX, XXX−XXX

(10) Zhu, Y.; Yang, B.; Liu, J.; Wang, X.; Wang, L.; Chen, X.; Yang, C. A flexible and biocompatible triboelectric nanogenerator with tunable internal resistance for powering wearable devices. *Sci. Rep.* **2016**, *6*, No. 22233. http://www.nature.com/articles/srep22233#supplementary-information.
(11) Fan, F.-R.; Lin, L.; Zhu, G.; Wu, W.; Zhang, R.; Wang, Z. L. Transparent Triboelectric Nanogenerators and Self-Powered Pressure Sensors Based on Micropatterned Plastic Films. *Nano Lett.* **2012**, *12*, 3109−3114.
(12) Jeong, C. K.; Baek, K. M.; Niu, S.; Nam, T. W.; Hur, Y. H.; Park, D. Y.; Hwang, G.-T.; Byun, M.; Wang, Z. L.; Jung, Y. S.; Lee, K. J. Topographically-Designed Triboelectric Nanogenerator via Block Copolymer Self-Assembly. *Nano Lett.* **2014**, *14*, 7031−7038.
(13) Kim, D.; Jeon, S.-B.; Kim, J. Y.; Seol, M.-L.; Kim, S. O.; Choi, Y.-K. High-performance nanopattern triboelectric generator by block copolymer lithography. *Nano Energy* **2015**, *12*, 331−338.
(14) Zhang, X.-S.; Han, M.-D.; Wang, R.-X.; Meng, B.; Zhu, F.-Y.; Sun, X.-M.; Hu, W.; Wang, W.; Li, Z.-H.; Zhang, H.-X. High-performance triboelectric nanogenerator with enhanced energy density based on single-step fluorocarbon plasma treatment. *Nano Energy* **2014**, *4*, 123−131.
(15) Lee, K. Y.; Chun, J.; Lee, J.-H.; Kim, K. N.; Kang, N.-R.; Kim, J.-Y.; Kim, M. H.; Shin, K.-S.; Gupta, M. K.; Baik, J. M.; Kim, S.-W. Hydrophobic Sponge Structure-Based Triboelectric Nanogenerator. *Adv. Mater.* **2014**, *26*, 5037−5042.
(16) Kim, D.; Park, S.-J.; Jeon, S.-B.; Seol, M.-L.; Choi, Y.-K. A Triboelectric Sponge Fabricated from a Cube Sugar Template by 3D Soft Lithography for Superhydrophobicity and Elasticity. *Adv. Electron. Mater.* **2016**, *2*, No. 1500331.
(17) Chen, J.; Guo, H.; He, X.; Liu, G.; Xi, Y.; Shi, H.; Hu, C. Enhancing Performance of Triboelectric Nanogenerator by Filling High Dielectric Nanoparticles into Sponge PDMS Film. *ACS Appl. Mater. Interfaces* **2016**, *8*, 736−744.
(18) Chun, J.; Kim, J. W.; Jung, W.-s.; Kang, C.-Y.; Kim, S.-W.; Wang, Z. L.; Baik, J. M. Mesoporous pores impregnated with Au nanoparticles as effective dielectrics for enhancing triboelectric nanogenerator performance in harsh environments. *Energy Environ. Sci.* **2015**, *8*, 3006−3012.
(19) Lerf, A.; He, H.; Forster, M.; Klinowski, J. Structure of Graphite Oxide Revisited. *J. Phys. Chem. B* **1998**, *102*, 4477−4482.
(20) Que, R.; Shao, Q.; Li, Q.; Shao, M.; Cai, S.; Wang, S.; Lee, S.-T. Flexible Nanogenerators Based on Graphene Oxide Films for Acoustic Energy Harvesting. *Angew. Chem., Int. Ed.* **2012**, *51*, 5418−5422.
(21) Tian, H.; Ma, S.; Zhao, H.-M.; Wu, C.; Ge, J.; Xie, D.; Yang, Y.; Ren, T.-L. Flexible electrostatic nanogenerator using graphene oxide film. *Nanoscale* **2013**, *5*, 8951−8957.
(22) Huang, T.; Lu, M.; Yu, H.; Zhang, Q.; Wang, H.; Zhu, M. Enhanced Power Output of a Triboelectric Nanogenerator Composed of Electrospun Nanofiber Mats Doped with Graphene Oxide. *Sci. Rep.* **2015**, *5*, No. 13942. http://www.nature.com/articles/srep13942#supplementary-information.
(23) Islam, R.; Papathanassiou, A. N.; Chan Yu King, R.; Brun, J.-F.; Roussel, F. Evidence of interfacial charge trapping mechanism in polyaniline/reduced graphene oxide nanocomposites. *Appl. Phys. Lett.* **2015**, *107*, No. 053102.
(24) Wang, Z.; Nelson, J. K.; Hillborg, H.; Zhao, S.; Schadler, L. S. Graphene Oxide Filled Nanocomposite with Novel Electrical and Dielectric Properties. *Adv. Mater.* **2012**, *24*, 3134−3137.
(25) Yang, B.; Zeng, W.; Peng, Z.-H.; Liu, S.-R.; Chen, K.; Tao, X.-M. A Fully Verified Theoretical Analysis of Contact-Mode Triboelectric Nanogenerators as a Wearable Power Source. *Adv. Energy Mater.* **2016**, *6*, No. 1600505.
(26) Hummers, W. S.; Offeman, R. E. Preparation of Graphitic Oxide. *J. Am. Chem. Soc.* **1958**, *80*, 1339.
(27) Bai, Y.; Rakhi, R. B.; Chen, W.; Alshareef, H. N. Effect of pH-induced chemical modification of hydrothermally reduced graphene oxide on supercapacitor performance. *J. Power Sources* **2013**, *233*, 313−319.
(28) Ikjoo, B.; Anthony, W. C.; Beomjoon, K. Transfer of thin Au films to polydimethylsiloxane (PDMS) with reliable bonding using (3-mercaptopropyl)trimethoxysilane (MPTMS) as a molecular adhesive. *J. Micromech. Microeng.* **2013**, *23*, No. 085016.
(29) Kaniyoor, A.; Ramaprabhu, S. A Raman spectroscopic investigation of graphite oxide derived graphene. *AIP Adv.* **2012**, *2*, No. 032183.
(30) Tuinstra, F.; Koenig, J. L. Raman Spectrum of Graphite. *J. Chem. Phys.* **1970**, *53*, 1126−1130.
(31) Stankovich, S.; Dikin, D. A.; Piner, R. D.; Kohlhaas, K. A.; Kleinhammes, A.; Jia, Y.; Wu, Y.; Nguyen, S. T.; Ruoff, R. S. Synthesis of graphene-based nanosheets via chemical reduction of exfoliated graphite oxide. *Carbon* **2007**, *45*, 1558−1565.
(32) King, A. A. K.; Davies, B. R.; Noorbehesht, N.; Newman, P.; Church, T. L.; Harris, A. T.; Razal, J. M.; Minett, A. I. A New Raman Metric for the Characterisation of Graphene oxide and its Derivatives. *Sci. Rep.* **2016**, *6*, No. 19491.
(33) Ambrosi, A.; Bonanni, A.; Sofer, Z.; Cross, J. S.; Pumera, M. Electrochemistry at Chemically Modified Graphenes. *Chem. - Eur. J.* **2011**, *17*, 10763−10770.
(34) Kundu, S.; Wang, Y.; Xia, W.; Muhler, M. Thermal Stability and Reducibility of Oxygen-Containing Functional Groups on Multiwalled Carbon Nanotube Surfaces: A Quantitative High-Resolution XPS and TPD/TPR Study. *J. Phys. Chem. C* **2008**, *112*, 16869−16878.
(35) Gupta, B.; Kumar, N.; Panda, K.; Kanan, V.; Joshi, S.; Visoly-Fisher, I. Role of oxygen functional groups in reduced graphene oxide for lubrication. *Sci. Rep.* **2017**, *7*, No. 45030. https://www.nature.com/articles/srep45030#supplementary-information.
(36) Yaqoob, U.; Uddin, A. S. M. I.; Chung, G.-S. The effect of reduced graphene oxide on the dielectric and ferroelectric properties of PVDF-BaTiO3 nanocomposites. *RSC Adv.* **2016**, *6*, 30747−30754.
(37) Xia, X.; Chen, J.; Liu, G.; Javed, M. S.; Wang, X.; Hu, C. Aligning graphene sheets in PDMS for improving output performance of triboelectric nanogenerator. *Carbon* **2017**, *111*, 569−576.
(38) Yuan, J.; Luna, A.; Neri, W.; Zakri, C.; Schilling, T.; Colin, A.; Poulin, P. Graphene liquid crystal retarded percolation for new high-k materials. *Nat. Commun.* **2015**, *6*, No. 8700.
(39) Stankovich, S.; Dikin, D. A.; Dommett, G. H. B.; Kohlhaas, K. M.; Zimney, E. J.; Stach, E. A.; Piner, R. D.; Nguyen, S. T.; Ruoff, R. S. Graphene-based composite materials. *Nature* **2006**, *442*, 282−286.
(40) Glover, A. J.; Adamson, D. H.; Schniepp, H. C. Charge-Driven Selective Adsorption of Sodium Dodecyl Sulfate on Graphene Oxide Visualized by Atomic Force Microscopy. *J. Phys. Chem. C* **2012**, *116*, 20080−20085.
(41) Hsieh, A. G.; Korkut, S.; Punckt, C.; Aksay, I. A. Dispersion Stability of Functionalized Graphene in Aqueous Sodium Dodecyl Sulfate Solutions. *Langmuir* **2013**, *29*, 14831−14838.
(42) Hsieh, A. G.; Punckt, C.; Korkut, S.; Aksay, I. A. Adsorption of Sodium Dodecyl Sulfate on Functionalized Graphene Measured by Conductometric Titration. *J. Phys. Chem. B* **2013**, *117*, 7950−7958.
(43) Tummala, N. R.; Grady, B. P.; Striolo, A. Lateral confinement effects on the structural properties of surfactant aggregates: SDS on graphene. *Phys. Chem. Chem. Phys.* **2010**, *12*, 13137−13143.
(44) Onogi, Y.; Sugiura, N.; Matsuda, C. Temperature Effect on Dissipation of Triboelectric Charge into Air from Textile Surfaces. *Text. Res. J.* **1997**, *67*, 45−49.
(45) Niu, S.; Wang, S.; Lin, L.; Liu, Y.; Zhou, Y. S.; Hu, Y.; Wang, Z. L. Theoretical study of contact-mode triboelectric nanogenerators as an effective power source. *Energy Environ. Sci.* **2013**, *6*, 3576−3583.
(46) Wang, S.; Xie, Y.; Niu, S.; Lin, L.; Liu, C.; Zhou, Y. S.; Wang, Z. L. Maximum Surface Charge Density for Triboelectric Nanogenerators Achieved by Ionized-Air Injection: Methodology and Theoretical Understanding. *Adv. Mater.* **2014**, *26*, 6720−6728.
(47) Wang, J.; Wu, C.; Dai, Y.; Zhao, Z.; Wang, A.; Zhang, T.; Wang, Z. L. Achieving ultrahigh triboelectric charge density for efficient energy harvesting. *Nat. Commun.* **2017**, *8*, No. 88.

DOI: 10.1021/acsami.8b02495
ACS Appl. Mater. Interfaces XXXX, XXX, XXX−XXX